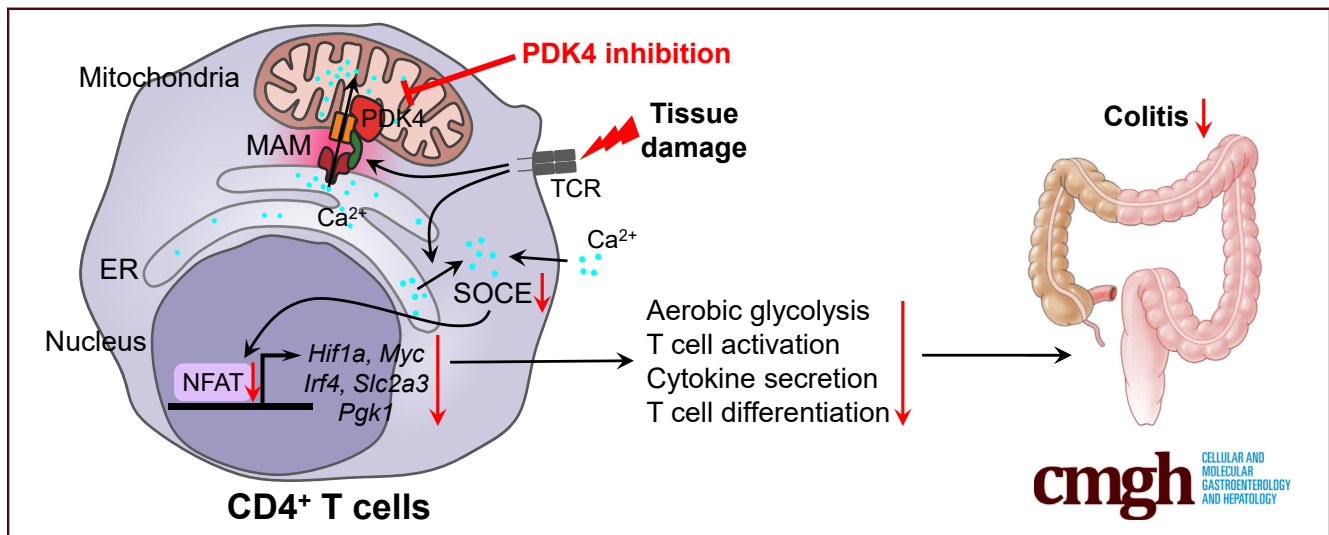


ORIGINAL RESEARCH

Inhibition of Pyruvate Dehydrogenase Kinase 4 in CD4⁺ T Cells Ameliorates Intestinal Inflammation

Hoyul Lee,^{1,*} Jae Han Jeon,^{1,2,*} Yu-Jeong Lee,³ Mi-Jin Kim,¹ Woong Hee Kwon,⁴ Dipanjan Chanda,¹ Themis Thoudam,¹ Haushabhau S. Pagire,⁵ Suvarna H. Pagire,⁵ Jin Hee Ahn,⁵ Robert A. Harris,⁶ Eun Soo Kim,^{7,§} and In-Kyu Lee^{1,8,§}

¹Research Institute of Aging and Metabolism, Kyungpook National University, Daegu, Republic of Korea; ²Department of Internal Medicine, School of Medicine, Kyungpook National University, Kyungpook National University Chilgok Hospital, Daegu, Republic of Korea; ³Cell & Matrix Research Institute, Kyungpook National University, Daegu, Republic of Korea; ⁴Leading-Edge Research Center for Drug Discovery and Development for Diabetes and Metabolic Disease, Kyungpook National University Hospital, Daegu, Republic of Korea; ⁵Department of Chemistry, Gwangju Institute of Science and Technology, Gwangju, Republic of Korea; ⁶Department of Biochemistry and Molecular Biology, University of Kansas Medical Center, Kansas City, Kansas; ⁷Division of Gastroenterology, Department of Internal Medicine, Kyungpook National University, Kyungpook National University Hospital, Daegu, Republic of Korea; and ⁸Department of Internal Medicine, School of Medicine, Kyungpook National University, Kyungpook National University Hospital, Daegu, Republic of Korea



SUMMARY

Metabolic reprogramming and calcium signaling are critical to pathogenic CD4⁺ T cells. Here, we demonstrate that PDK4 deletion mitigates aerobic glycolysis and calcium signaling by hindering mitochondria-associated membranes in activated CD4⁺ T cells. Consequently, PDK4 inhibition attenuates colitis in mice.

BACKGROUND & AIMS: Despite recent evidence supporting the metabolic plasticity of CD4⁺ T cells, it is uncertain whether the metabolic checkpoint pyruvate dehydrogenase kinase (PDK) in T cells plays a role in the pathogenesis of colitis.

METHODS: To investigate the role of PDK4 in colitis, we used dextran sulfate sodium (DSS)-induced colitis and T-cell transfer colitis models based on mice with constitutive knockout (KO) or CD4⁺ T-cell-specific KO of PDK4 (*Pdk4*^{fl/fl}CD4^{Cre}). The effect

of PDK4 deletion on T-cell activation was also studied in vitro. Furthermore, we examined the effects of a pharmacologic inhibitor of PDK4 on colitis.

RESULTS: Expression of PDK4 increased during colitis development in a DSS-induced colitis model. Phosphorylated PDHE1 α , a substrate of PDK4, accumulated in CD4⁺ T cells in the lamina propria of patients with inflammatory bowel disease. Both constitutive KO and CD4⁺ T-cell-specific deletion of PDK4 delayed DSS-induced colitis. Adoptive transfer of PDK4-deficient CD4⁺ T cells attenuated murine colitis, and PDK4 deficiency resulted in decreased activation of CD4⁺ T cells and attenuated aerobic glycolysis. Mechanistically, there were fewer endoplasmic reticulum-mitochondria contact sites, which are responsible for inter-organelle calcium transfer, in PDK4-deficient CD4⁺ T cells. Consistent with this, GM-10395, a novel inhibitor of PDK4, suppressed T-cell activation by reducing endoplasmic reticulum-mitochondria calcium transfer, thereby ameliorating murine colitis.

CONCLUSIONS: PDK4 deletion from CD4⁺ T cells mitigates colitis by metabolic and calcium signaling modulation, suggesting PDK4 as a potential therapeutic target for IBD. (*Cell Mol Gastroenterol Hepatol* 2023;15:439–461; <https://doi.org/10.1016/j.jcmgh.2022.09.016>)

Keywords: Inflammatory Bowel Disease; Pyruvate Dehydrogenase Kinase; Mitochondria-Associated ER Membrane.

Inflammatory bowel disease (IBD), which comprises Crohn's disease (CD) and ulcerative colitis (UC), is a chronic inflammatory condition of the gastrointestinal tract. Although the exact pathophysiology remains unclear, it appears to be associated with aberrant adaptive immune responses in genetically susceptible hosts.¹ Intestinal CD4⁺ T cells are central mediators of intestinal immune homeostasis and inflammation.^{2,3} IBD patients with active disease have a higher percentage of CD4⁺ T cells in the intestine than healthy controls or patients with inactive IBD, suggesting an essential role for CD4⁺ T cells in the pathogenesis of IBD.⁴

In recent years, our understanding of the relationship between the T-cell metabolic machinery and immune function has increased; for example, we now know that the metabolic reliance of T cells on oxidative phosphorylation (OXPHOS) and glycolysis differs according to activity status. Naive T cells are metabolically inert and use OXPHOS primarily, whereas activated T cells skew their metabolic programs toward glycolysis to meet the metabolic demands of proliferation, differentiation, and effector functions.^{5,6} Emerging evidence shows that modulating metabolism affects the responses of inflammatory cells.⁷

Rapid transition of metabolic programming to aerobic glycolysis can be achieved by triggering of calcium signaling pathways during early T-cell activation. In general, T-cell receptor (TCR)-induced T-cell activation stimulates the inositol trisphosphate receptor (IP3R) on the endoplasmic reticulum (ER) membrane, resulting in release of calcium from the ER. The reduced reservoir of ER calcium triggers activation of stromal interaction molecule 1 (STIM1) on the ER membrane. Activated STIM1 binds to the Orai1 plasma membrane calcium channel and induces calcium influx. Amplified cytosolic calcium prompts calcineurin-mediated dephosphorylation of nuclear factor of an activated T cell (NFAT). Activated NFAT translocates to the nucleus and promotes transcriptional expression of genes associated with T-cell immune responses,⁸ including those that regulate glycolytic enzymes and cytokines. The store-operated calcium entry (SOCE) and calcium signaling pathways appear to be essential for T-cell-mediated immunity and metabolic reprogramming.^{9–11} Indeed, disturbance of calcium channel activity in CD4⁺ T cells attenuates disease severity and intestinal inflammation in an experimental model of colitis.^{10–13}

Pyruvate dehydrogenase E1 α (PDHE1 α), one component of the pyruvate dehydrogenase complex, plays a critical role in promoting OXPHOS in mitochondria.^{14–16} Pyruvate dehydrogenase kinase (PDK), which comprises 4 different


isoenzymes (PDK1 to PDK4), inhibits the pyruvate dehydrogenase complex phosphorylating PDHE1 α , resulting in increased aerobic glycolysis.¹⁷ During the last decade, we demonstrated that aberrant expression of PDKs has a positive association with pathologic conditions such as obesity, diabetes, cancer, and inflammation, and that inhibition of PDKs has a therapeutic effect on such diseases.^{15,16,18–26}

Recently, we identified a novel role for PDK4 in reinforcing the mitochondria-associated membrane (MAM) microdomain^{27,28} between the ER and mitochondria in skeletal muscle,¹⁹ suggesting a potential interaction between PDK4 and the MAM in immune cells. This sub-organelle structure is responsible for transferring calcium from the ER to mitochondria via a MAM-residing voltage-dependent anion channel (VDAC)/IP3R/glucose-regulated protein 75 complex, thereby affecting mitochondrial respiration.²⁹ In effector memory CD8⁺ T cells, the MAM structure is enriched markedly compared with that in naive CD8⁺ T cells. Inhibition of MAM in activated effector memory CD8⁺ T cells impairs mitochondrial respiration and cytokine secretion.³⁰ However, the contribution of PDK4 to T-cell activation, metabolism, MAM structure, and calcium signaling in CD4⁺ T cells has not been investigated.

Here, we show increased PDK4 and p-PDHE1 α expression in T cells infiltrating the colonic lamina propria (LP) of patients with IBD and in the LP of dextran sulfate sodium (DSS)-challenged mice. Genetic and pharmacologic inhibition of PDK4 prevented DSS-induced colitis. Of note, ablation of PDK4 in CD4⁺ T cells, but not in intestinal epithelial cells (IEC), is required for amelioration of colitis. In vitro studies revealed that PDK4-deficient CD4⁺ T cells were less activated than wild-type (WT) CD4⁺ T cells. In addition, PDK4 deficiency restored the Th17/Treg balance both in vitro and in vivo. Mechanistically, PDK4 ablation led to bioenergetic dysfunction, accompanied by decreased MAM formation/interorganelle calcium transfer and decreased aerobic glycolysis/mechanistic target of rapamycin (mTOR)

*Authors share co-first authorship; §Authors share co-senior authorship.

Abbreviations used in this paper: ATP, adenosine triphosphate; CD, Crohn's disease; DEG, differentially expressed gene; DSS, dextran sodium sulfate; ECAR, extracellular acidification rate; ELISA, enzyme-linked immunosorbent assay; ER, endoplasmic reticulum; GSEA, Gene Set Enrichment Analysis; IBD, inflammatory bowel disease; IEC, intestinal epithelial cells; IFN, interferon; IHC, immunohistochemistry; IL, interleukin; IP3R, inositol trisphosphate receptor; KO, knockout; LP, lamina propria; MAM, mitochondria-associated membrane; mTOR, mechanistic target of rapamycin; NFAT, nuclear factor of an activated T cell; OCR, oxygen consumption rate; OXPHOS, oxidative phosphorylation; PBS, phosphate-buffered saline; PCR, polymerase chain reaction; PDHE1 α , pyruvate dehydrogenase E1 α ; PDK, pyruvate dehydrogenase kinase; SOCE, store-operated calcium entry; STIM1, stromal interaction molecule 1; TCR, T-cell receptor; TNF, tumor necrosis factor; UC, ulcerative colitis; VDAC, voltage-dependent anion channel; WT, wild-type.

 Most current article

© 2022 The Authors. Published by Elsevier Inc. on behalf of the AGA Institute. This is an open access article under the CC BY-NC-ND license (<http://creativecommons.org/licenses/by-nc-nd/4.0/>).

2352-345X

<https://doi.org/10.1016/j.jcmgh.2022.09.016>

signaling pathway activation in CD4⁺ T cells, leading to suppression of T-cell activation and effector functions.

Results

Increased Expression of PDK4 by Colitogenic CD4⁺ T Cells From Humans and Mice

To identify the PDK isoform responsible for intestinal inflammation, we first examined the effect of DSS-induced inflammation on expression of PDK in mouse colon. DSS administration led to a significant time-dependent increase in colonic expression of PDK4, as well as enhanced PDHE1 α phosphorylation (Figure 1A). This finding led us to focus on the role of PDK4 in the pathogenesis of IBD.

Immunohistochemistry (IHC) staining was performed to identify the location of phosphorylated PDHE1 α in tissue sections from mice at 6 days after DSS challenge. Although there was no difference in p-PDHE1 α expression in IECs between before and after DSS challenge, the level of p-PDHE1 α -positive cells was markedly higher in the severely inflamed LP (DSS-6d) than in the DSS-unchallenged LP (control) (Figure 1B).

Next, we profiled p-PDHE1 α -expressing cells using flow cytometry (Figure 1C). After DSS challenge, we found increased expression of p-PDHE1 α (Figure 1D). In line with the IHC staining results, there was no difference in p-PDHE1 α levels in nonhematopoietic cells (CD45⁻) at DSS0 or DSS6 (Figure 1F), whereas p-PDHE1 α levels were elevated in leukocytes (CD45⁺ cells) (Figure 1D); these data suggest that increased expression of p-PDHE1 α upon DSS challenge is a phenomenon confined to leukocytes. Colonic CD3⁺ T cells, neutrophils, and macrophages, but not dendritic cells, showed higher expression of p-PDHE1 α (Figure 1E and G), suggestive of overall immunometabolic reprogramming under inflammatory conditions. Under conditions of intestinal inflammation (DSS6), CD4⁺ T cells showed higher expression of p-PDHE1 α than under physiological conditions (DSS0) (Figure 1E). However, altered expression in CD8⁺ T cells was not as prominent (Figure 1E).

Consistent with these findings, IHC staining clearly showed that expression of PDK4/p-PDHE1 α (Figure 2A and B) was markedly enriched in the LP, but not in the IEC, of inflamed tissue from patients with IBD. This suggests that infiltrating immune cells are likely to be responsible for augmented expression of PDK4/p-PDHE1 α in the inflamed area. Because aberrant activation of CD4⁺ T cells and macrophages is the key contributor to the pathogenesis of IBD,³¹ we hypothesized that altered expression of PDK4/p-PDHE1 α would be associated with accumulation of macrophages or CD4⁺ T cells in the gut. Therefore, we performed co-immunofluorescence staining of inflamed biopsy tissue collected from patients with IBD and from healthy controls to determine which infiltrating immune cells express p-PDHE1 α under inflammatory conditions (Figure 2C and D). In normal controls, the percentage of p-PDHE1 α -positive CD4⁺ T cells was significantly higher than that of CD64⁺ macrophages (Figure 2E), suggesting that CD4⁺ T cells are the likely source of augmented PDK expression. Moreover, the p-PDHE1 α -expressing CD4⁺ T-cell population was significantly enriched in inflamed biopsy tissue from patients with IBD

when compared with that in controls (Figure 2C). Expression of phosphorylated PDHE1 α in macrophages from patients with IBD was not different from that in the normal control (Figure 2D), despite augmented expression of p-PDHE1 α by macrophages under conditions of intestinal inflammation observed in the murine colitis model (Figure 1G). Collectively, these results highlight the colitogenic role of the PDK4/p-PDHE1 α axis in CD4⁺ T cells during intestinal inflammation in both patients with IBD and mouse colitis models.

PDK4-Deficient Mice Are Protected From DSS-Induced Colitis

Next, we tested the anticolitic effects of PDK4 deficiency in a DSS-treated colitis mouse model. Before induction of experimental colitis, we confirmed that colonic IEC from PDK4 KO mice display normal histology, proliferation, and apoptosis (Figure 3A–C). Specific gene expression of IEC markers *Reg3g* (Paneth cells), *Muc1* and *Muc2* (goblet cells), *Kit* (crypt cells), and *Lgr5* (stem cells) in PDK4 KO mice was also comparable with that in WT mice (Figure 3D and E).

Next, we challenged WT or PDK4 KO mice with DSS. PDK4 KO mice lost less weight than WT mice upon DSS challenge (Figure 4A). Also, disease was less severe in PDK4 KO mice (Figure 4B). Histologic analysis revealed that WT mice exhibited extensive loss of the epithelial lining, accompanied by severe inflammation of the LP, whereas PDK4 KO mice showed a relatively well-retained intestinal epithelial layer and minimal infiltration of the LP by inflammatory cells (Figure 4C and D). The colon length in PDK4 KO mice was better preserved than that in WT mice (Figure 4E and F). In addition, DSS-induced intestinal permeability was attenuated in PDK4 KO mice (Figure 4G). We also observed down-regulation of mRNA encoding cytokines (*Ifng*, *Il1b*, and *Il6*) in the colon of PDK4 KO mice (Figure 4H). These data clearly show that PDK4 KO mice are resistant to colitis.

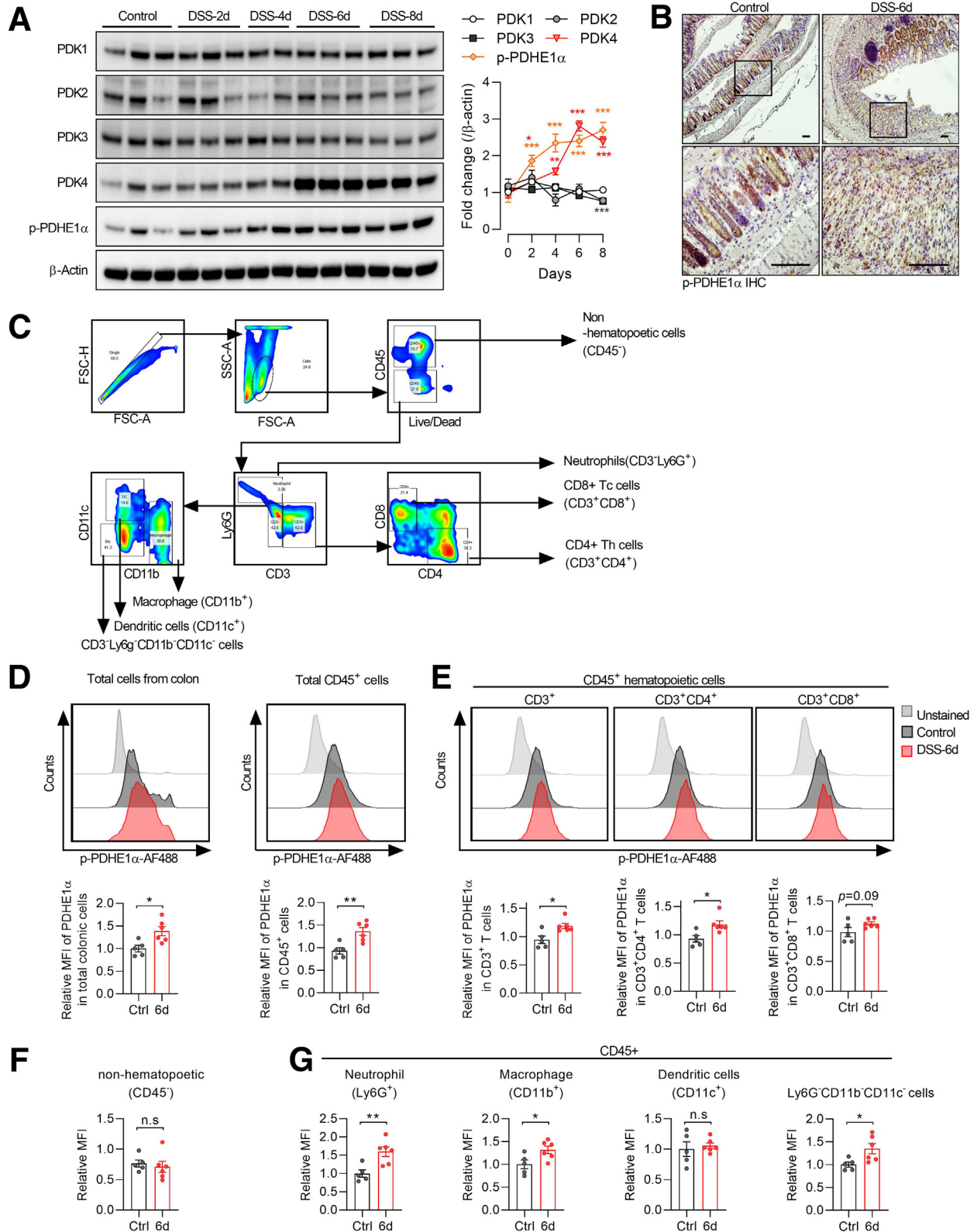
Flow cytometry analysis (Figure 4I) revealed that PDK4 deletion reduced the absolute number and percentage of CD4⁺ T cells significantly (Figure 4J), including Th1 (interferon gamma [IFN- γ] secreting) and Th17 (interleukin [IL] 17 α secreting) cells in the LP (Figure 4K). By contrast, the numbers of immunosuppressive Treg cells in PDK4 KO mice increased significantly (Figure 4K). Colonic cytokine production (IFN- γ , IL1, IL12, IL17, and tumor necrosis factor alpha [TNF- α]) was reduced in response to colitis during ex vivo organ culture (Figure 4L). Taken together, these findings suggest that PDK4 deficiency protects mice against DSS-induced colitis.

CD4⁺ T-Cell-Specific PDK4-Deficient Mice Are Protected From DSS-Induced Colitis

Next, we used a CD4⁺ T-cell-specific PDK4 KO mouse (PDK4^{CD4}) model to show that PDK4 deficiency-mediated protection against DSS-induced colitis is regulated by CD4⁺ T cells (Figure 5A–C). As observed in PDK4 KO mice, PDK4^{CD4} mice showed significant attenuation of DSS-induced colitis, as judged by less weight loss, lower disease severity scores, and milder sequelae on histologic

analysis (Figure 5D–G). We observed marked infiltration of the LP by immune cells, as well as loss of IEC, in WT mice; these pathologies were profoundly attenuated in PDK4^{CD4}

mice (Figure 5G). Furthermore, colon length and intestinal barrier function (Figure 5H–J) were better in PDK4^{CD4} mice than in WT controls. Expression of mRNA encoding all



proinflammatory cytokines (*Ifng*, *Il1b*, *Il6*, *Il12b*, *Il17a*, and *Tnfa*) tested in this study was attenuated in PDK4^{CD4} mice (Figure 5K). Flow cytometry analysis (Figure 5L) revealed that the total number of LP CD4⁺ T cells in PDK4^{CD4} mice was significantly lower than that in WT mice (Figure 5M), and that PDK4^{CD4} mice had lower percentages of Th1 and Th17 (Figure 5N). By contrast, PDK4^{CD4} mice had higher numbers of immunosuppressive Tregs than WT controls (Figure 5M). Inflamed colon tissues from PDK4^{CD4} mice secreted substantially lower amounts of cytokines (IL1, IL12, IL17, and TNF- α) than the control (Figure 5O). Collectively, these data suggest that expression of PDK4 in CD4⁺ T cells is required for development of DSS-induced colitis.

PDK4 Deletion From IEC Does Not Protect Against Experimental Colitis

To rule out the possibility that PDK4 deficiency in IECs contributes to protection against intestinal inflammation despite its redundant role in IECs under normal conditions (Figure 3), we challenged mice lacking PDK4 specifically in IECs (PDK4^{villin}) (Figure 6A and B) with DSS. Weight loss and disease severity scores after DSS challenge were similar between DSS-treated and control mice (Figure 6C and D). Histologic analysis revealed that inflammation was comparable between the test and control groups (Figure 6E and F). Although colon length was modestly shorter in PDK4^{villin} mice (Figure 6G and H), DSS-induced intestinal permeability (Figure 6I) was not different between groups. These observations indicate that PDK4 in IECs plays a dispensable role in pathogenesis of colitis.

PDK4-deficient T Cells Ameliorate Adoptive T-Cell Transfer Colitis

Because the chemically induced colitis model has limitations with respect to the pathologic mechanisms that cause human disease, as well as colitis-associated gene expression,³² we adoptively transferred natural Treg-depleted naive CD4⁺ T cells (CD4⁺CD45RB^{hi}CD25⁻) from WT or PDK4 KO mice to *Rag1*^{-/-} recipient mice. These mice, which lack Treg cells, are prone to developing colitis spontaneously.^{33,34}

Unlike mice receiving WT T cells, mice injected with PDK4 KO naive T cells developed less severe colitis, as assessed by weight changes and disease severity scores (Figure 7A and B). Histologic examination revealed a near absence of inflammation in PDK4 KO T-cell-transferred mice (Figure 7C and D). Despite comparable colon lengths

(Figure 7E and F), in vivo intestinal permeability was also significantly less severe in these mice (Figure 7G). Expression of mRNA encoding cytokines *Il1b*, *Il12*, and *Il17a* in the colon was significantly lower in PDK4 KO T-cell-transferred mice (Figure 7H).

Flow cytometry analysis (Figure 7I) indicated that the number of PDK4 KO CD4⁺ T cells in the LP was lower than that in control mice, whereas the percentage of CD4⁺ within the CD3⁺ T-cell population was comparable, suggesting that PDK4 is likely important for intestinal homing (Figure 7J). The percentage of Th1 and Th17 cells in the LP of mice receiving PDK4 KO T cells was significantly lower than that in controls (Figure 7K), whereas the percentage of iTregs in the LP of PDK4 KO T-cell-transferred mice was higher than that in the controls (Figure 7K), despite the absence of adoptive natural Treg cells. Cytokine production (IL1, IL12, and IL17) by ex vivo colon explant cultures was significantly down-regulated (Figure 7L).

Because PDK4-deficient naive CD4⁺ T cells failed to induce intestinal inflammation, we assessed the reconstitution of CD4⁺ T cells in lymphoid organs in *Rag1*^{-/-} mice. Flow cytometry analysis revealed a comparable distribution of CD3⁺ T cells and CD4⁺ T cells in spleen and mesenteric lymph nodes (Figure 7M and N) between WT and PDK4 KO T-cell-transferred mice, which indicates intact cell survival and lymphoid tissue homing in vivo. These results demonstrate that protection from colitis mediated by PDK4-deficient naive CD4⁺ T cells was due to diminished local immune responses in the gut. Taken together, the results indicate that CD4-specific PDK4 deficiency is sufficient to trigger anticolitogenic mechanisms in mice without disturbing immune integrity in other organs.

PDK4 Deficiency Suppresses T-Cell Activation and Th17 Differentiation

To gain insight into the molecular mechanisms underlying the anticolitic effects of PDK4 ablation, we measured expression of PDKs in activated CD4⁺ T cells (Figure 8A and B). Unstimulated basal PDK4 protein levels were relatively low but peaked after 2 hours of activation, whereas PDK2 was suppressed, and PDK3 reached a peak at a later time (48 hours) (Figure 8A). *Pdk4* transcription peaked at 4 hours after activation, whereas *pdk3* transcription increased at a later time (Figure 8B). Publicly available CD4⁺ T-cell activation RNA-sequencing data from the GEO database (GSE96538) also revealed increased *pdk4* transcription at 2

Figure 1. (See previous page). PDK4 or p-PDHE1 α is enriched in CD4⁺ T cells from a mouse model of DSS-induced colitis. (A and B) WT mice received 2.5% DSS in drinking water for 0, 2, 4, 6, or 8 days. The experiment was repeated twice. (A) Representative Western blots of PDK1-4, p-PDHE1 α , and β -actin expression in colon tissues (n = 2–3). (B) Representative images of immunohistochemistry staining of p-PDHE1 α in colon tissues from mice after treatment with DSS for 6 days (n = 3). Scale bar, 100 μ m. (C) Gating strategy used to examine expression of p-PDHE1 α in gut neutrophils, macrophages, dendritic cells, CD8⁺ T cells, and CD4⁺ T cells. (D–G) p-PDHE1 α levels in cells isolated from the colon of mice at day 0 (Ctrl) and day 6 (DSS-6d) of DSS treatment were analyzed by flow cytometry (n = 5, Ctrl; n = 6, DSS-6d). Expression of p-PDHE1 α by (D) CD45⁺ (hematopoietic cells) and (F) CD45⁻ (non-hematopoietic cells) in the lamina propria single-cell population isolated from DSS-treated mice. (E) CD3⁺ T cells were further gated into CD3⁺CD4⁺ and CD3⁺CD8⁺ T-cell populations. (G) Ly6G⁺ (neutrophils), CD11b⁺ (macrophages), CD11c⁺ (dendritic cells), and CD45⁺Ly6G⁻CD11b⁻CD11c⁻ cells. The experiment was repeated twice. Mean \pm standard error; *P < .05, **P < .01 (Student t test).

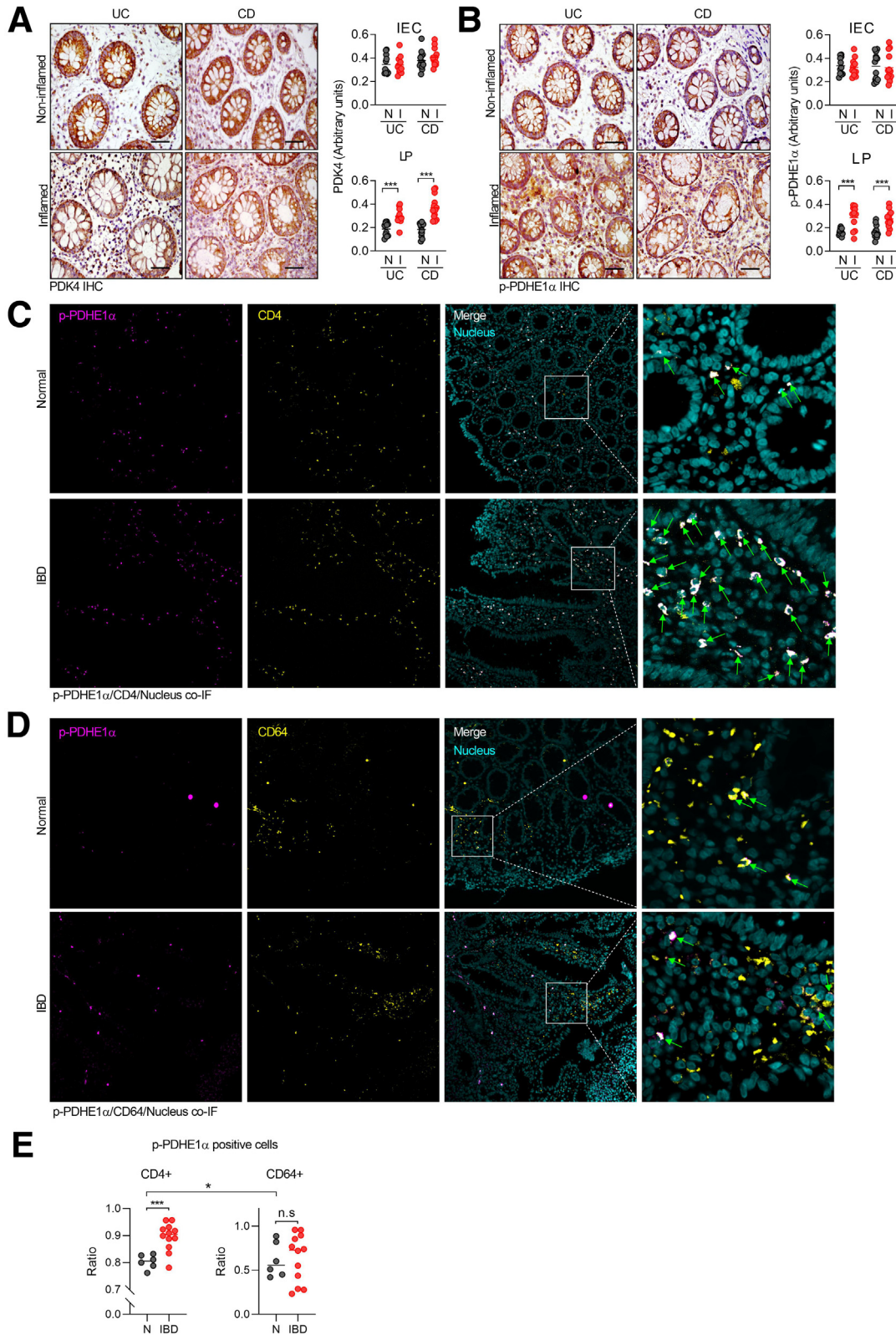


Figure 2. Augmented expression of p-PDHE1 α in lamina propria immune cells from patients with IBD. (A and B) Representative IHC staining of PDK4 and p-PDHE1 α in inflamed (I) or noninflamed (N) colonic biopsies from patients with CD (n = 13) and UC (n = 11). Scale bar, 100 μ m. (C and D) Co-immunofluorescence staining of p-PDHE1 α (magenta) and (C) CD4 (yellow) or (D) CD64 (yellow) in inflamed tissues from patients with IBD (n = 14) and controls (n = 6). Co-staining is indicated by green arrow. Nuclei are stained with DAPI (cyan). (E) Ratios of p-PDHE1 α -positive cells to CD4⁺ T cells and CD64⁺ macrophages. Mean \pm standard error; **P* < .05, ***P* < .01, ****P* < .001 (Student *t* test).

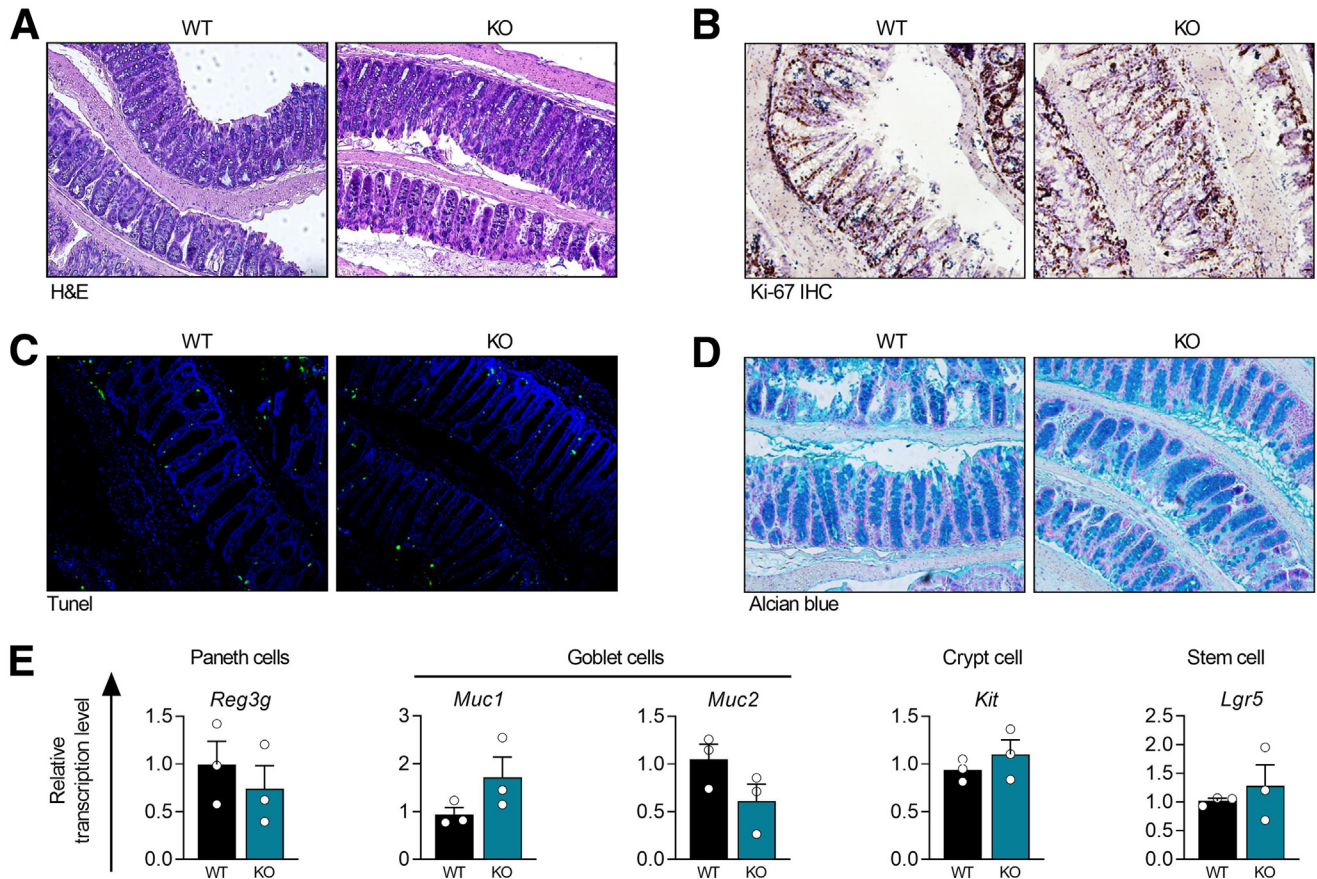


Figure 3. PDK4-deficient mice have normal colon epithelial functions. (A) Functions of intestinal epithelial cells (IECs) from PDK4-deficient mice were comparable with those of IECs from WT mice ($n = 3$). Representative images showing H&E staining of colon sections. (B) Representative immunohistochemistry images showing staining of Ki-67. (C) Representative images of TUNEL staining (green); nuclei are stained with DAPI (blue). (D) Representative images showing Alcian blue staining. (E) Expression of mRNA transcripts encoding *Reg3g* (Paneth cell marker), *Muc1* and *Muc2* (goblet cell markers), *Kit* (crypt cell marker), and *Lgr5* (stem cell marker). Mean \pm standard error; Student *t* test.

hours (Figure 8C),³⁵ which was consistent with our own data. These data illustrate that PDK4 is induced early during T-cell activation.

Next, we analyzed the gene expression profile in activated CD4⁺ T cells using unbiased RNA-sequencing. In total, 425 genes were differentially regulated, of which 215 were up-regulated and 210 were down-regulated, in PDK4 KO CD4⁺ T cells (Figure 8E). Notably, Gene Set Enrichment Analysis (GSEA) revealed that the calcium signaling pathway, inositol lipid mediated signaling, and PI3K signaling were down-regulated in PDK4 KO T cells (Figure 8D).

Because enrichment of lymphocyte activation was evident ($P = .03$) (Figure 8F), we examined whether PDK4 ablation affects activation of CD4⁺ T cells under Th0 conditions (Figure 8G). Because IL2 is a potent enhancer of T-cell function, we also tested whether IL2 production is a limiting factor. Consistent with this, we observed that PDK4 deficiency resulted in reduced T-cell activation (Figure 8G), as well as reduced cell granularity and size (Figure 8H and I). Secretion of proinflammatory cytokines (IFN- γ and IL17 α) decreased significantly under PDK4-deficient

conditions (Figure 8J), whereas cell viability, proliferation, and apoptosis were affected modestly by PDK4 deficiency (Figure 8K–M). Addition of exogenous IL2 restored neither T-cell activation (Figure 8G) nor IL17 α secretion (Figure 8J), suggesting that IL2 secretion is not a notable cause of T-cell activation.

Metabolic reprogramming toward aerobic glycolysis is a hallmark of T-cell activation.^{36,37} We found that PDK4 deficiency altered expression of glycolytic genes and mTOR signaling pathways in CD4⁺ T cells (Figure 9A–C), implying differential bioenergetics profiles. PDK4 KO CD4⁺ T cells had reduced basal glycolysis and glycolytic capacity (Figure 8D–F). At the same time, we observed decreased basal, maximal, and adenosine triphosphate (ATP)-linked oxygen consumption rate (OCR) and reserve capacity in PDK4-deficient CD4⁺ T cells (Figure 8G–K). Metabolic responsiveness to exogenous IL2 was significantly lower in PDK4-deficient CD4⁺ T cells (Figure 8D–K). Nevertheless, the degree of reduction in basal glycolysis was greater than that of basal OCR, resulting in a relatively higher OCR/extracellular acidification rate (ECAR) ratio (Figure 8L). Consistent with this, the increase in cytosolic lactate upon T-

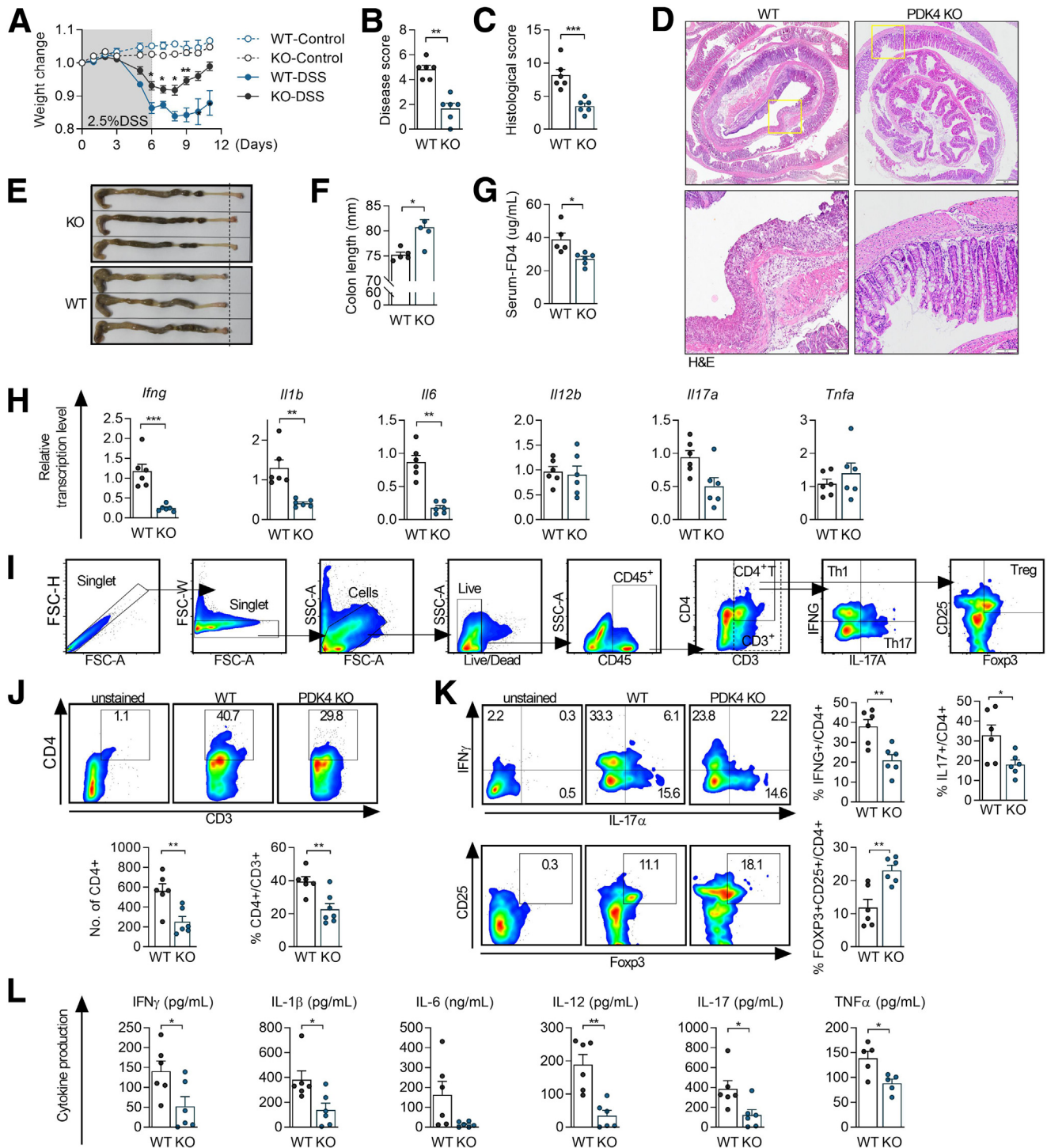


Figure 4. PDK4 deficiency protects against DSS-induced colitis. C57BL/6J PDK4 KO or WT mice received 2.5% DSS in drinking water for 6 days ($n = 6$). The experiment was repeated 3 times. (A) Weight changes. (B) Disease activity scores. (C) Histologic scores. (D) Representative H&E staining. Scale bars: upper, 500 μ m; lower, 100 μ m. (E) Gross image of the colon. (F) Colon length. (G) In vivo intestinal permeability test. (H) Relative levels of mRNA transcripts encoding *Ifng*, *Il1b*, *Il6*, *Il12b*, *Il17a*, and *Tnfa* in colon tissues ($n = 6$). (I) Gating strategy to identify Th1 (IFN- γ), Th17 (IL17 α), and Tregs (Foxp3⁺CD25⁺) cells. (J) Percentage of helper CD4⁺ T cells (CD4) among CD3⁺ T-cell population in the lamina propria was measured by flow cytometry. (K) Flow cytometry analysis of percentage of Th1 (IFN- γ), Th17 (IL17 α), and Treg (Foxp3⁺CD25⁺) cells among gut-infiltrating CD4⁺ T cells. (L) Ex vivo cytokine production (IFN- γ , IL1 β , IL6, IL12, IL17, and TNF- α) of colon organ cultures was measured by ELISA ($n = 6$). Mean \pm standard error; * $P < .05$, ** $P < .01$, *** $P < .001$ (Student t test).

cell activation was attenuated significantly in PDK4-deficient CD4⁺ T cells (Figure 8M), indicating reduced aerobic glycolysis. Despite addition of IL2, phosphorylation of ribosomal protein S6 (p-RPS6), a readout of mTOR signaling, was also attenuated (Figure 8N). Taken together, these findings suggest that deletion of PDK4 from CD4⁺ T cells rewires metabolism toward down-regulated mTOR signaling and reduced aerobic glycolysis.

Imbalance between effector T and regulatory T cells contributes to tissue damage during colitis. Therefore, we examined the ability of PDK4 KO naive CD4⁺ T cells to differentiate into Th1, Th2, Th17, and Treg cells. Although IFN- γ secretion by PDK4 KO CD4⁺ T cells activated under Th0 conditions was differentially regulated (Figure 7J), we did not observe any differences in Th1 differentiation (Figure 8O). Naive CD4⁺ T cells from both groups polarized into Th2 cells (Figure 8P). Notably, expression of IL17a by PDK4-deficient Th17 cells was significantly lower than that in the WT (Figure 8Q), whereas the proportion of Foxp3⁺CD25⁺ Tregs differentiated from PDK4 KO naive CD4⁺ T cells increased markedly (Figure 8R). Collectively, these observations demonstrate that inhibition of PDK4 suppresses T-cell effector functions and Th17/Treg differentiation.

Calcium Homeostasis and Metabolic Reprogramming in PDK4-Deficient CD4⁺ T Cells Are Impaired Through Disrupted MAM

Intracellular calcium flux is essential for lymphocyte activation; thus, any biological processes that impede calcium homeostasis can impact lymphocyte activation.^{12,36,38} RNA-sequencing analysis revealed that PDK4 deficiency led to compromised calcium signaling signatures (Figure 10A and B), including *Plcg2*, which is a key mediator that triggers SOCE (Figure 10B). To investigate whether PDK4 deletion affects calcium homeostasis, we induced SOCE by ER calcium depletion using ATP or α CD3.^{39,40} Deletion of PDK4 significantly and simultaneously compromised both SOCE and mitochondrial calcium levels in CD4⁺ T cells (Figure 10C–F).

One plausible hypothesis for altered calcium homeostasis in PDK4 KO CD4⁺ T cells is that PDK4 may reinforce MAM formation.¹⁹ Consistent with this hypothesis, co-immunofluorescence staining of disulfide isomerase and VDAC (markers of the ER and mitochondria, respectively) revealed less colocalization in PDK4 KO CD4⁺ T cells (Figure 10G). In situ proximity ligation assays, a more reliable tool for detecting MAM formation, showed that the interaction between MAM components VDAC1, IP3R, and GRP75 was compromised in PDK4 KO CD4⁺ T cells (Figure 10H and I). Next, we investigated formation of MAM in pathogenic CD4⁺ T cells of patients with UC. A proximity ligation assay revealed that MAM was significantly augmented in CD4⁺ T cells from patients with UC (Figure 10J). Therefore, we speculate that PDK4 inhibition may be useful to buffer pathogenic CD4⁺ T cells in both mouse and human pathogenic T cells via MAM disorganization.

SOCE and calcium signaling induce immediate calcineurin-mediated translocation of NFATc1.⁴¹ Therefore, we tested whether PDK4 deficiency impairs nuclear translocation of NFATc1 in T cells. The intensity of nuclear NFATc1 staining in PDK4-deficient CD4⁺ T cells was reduced markedly after TCR stimulation (Figure 10K). Accordingly, the transcription levels of transcriptional regulators (*Myc*, *Hif1a*, and *Irf4*) or glycolytic genes (*Slc2a3* and *Pgk1*) that bear NFAT-binding motifs in the regulatory regions⁴¹ were significantly down-regulated (Figure 10L). In line with this, secretion of IL2, which is transcriptionally regulated by NFAT, was markedly reduced in PDK4 KO T cells compared with the control (Figure 10M). Collectively, these data demonstrate that PDK4 seems to regulate metabolic reprogramming in pathogenic CD4⁺ T cells via MAM/SOCE/calcium signaling pathways and NFATc1-dependent transcriptional expression of glycolytic genes.

Small Molecule Targeting of PDK4 Prevents DSS-Induced Colitis

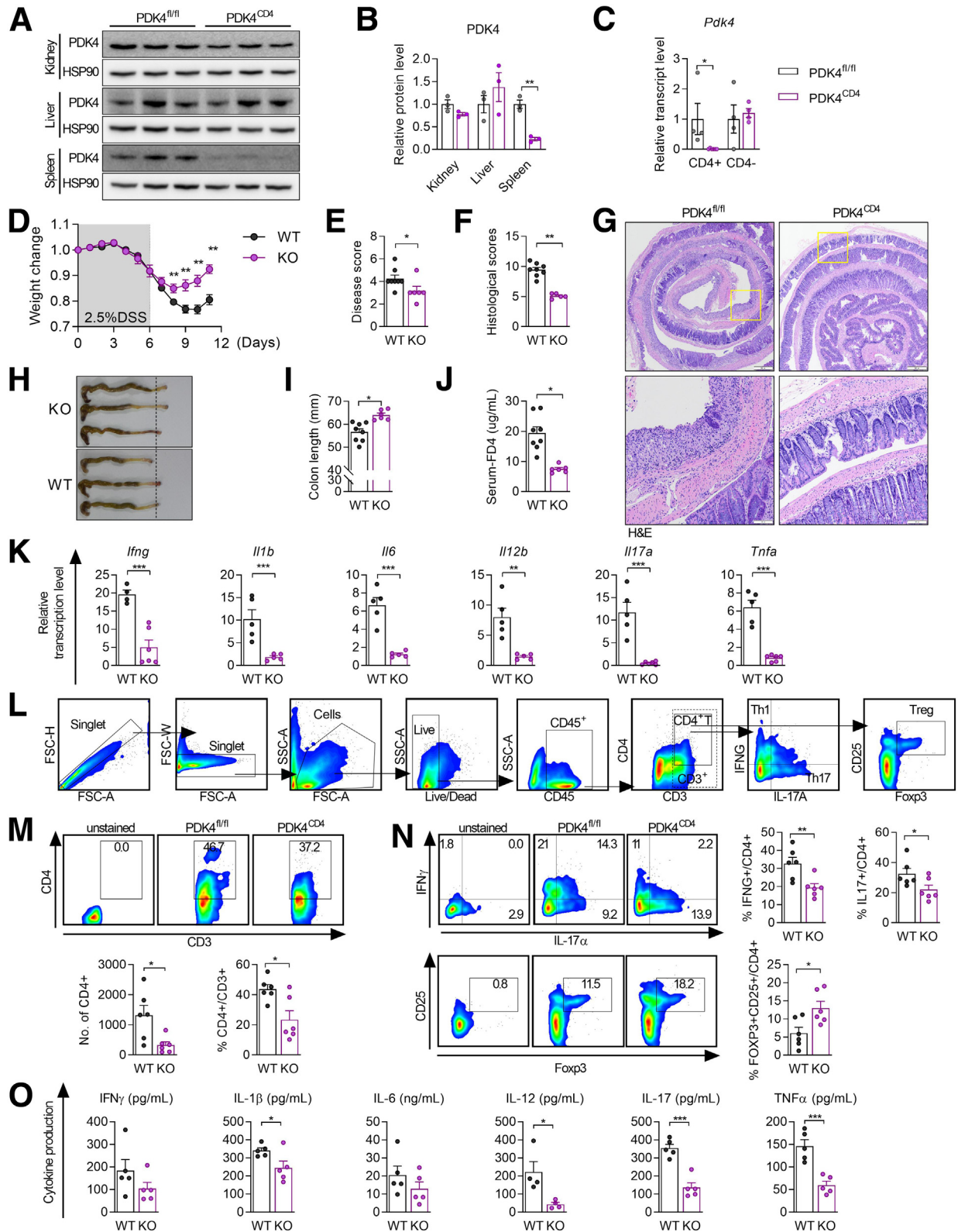
Recently, we synthesized a novel small molecule, GM-10395, that targets PDK4. This compound successfully dephosphorylated PDHE1 α in a dose-dependent manner, thereby suppressing PDK4 activity in CD4⁺ T cells (Figure 11A). PDK4 inhibition by GM-10395 decreased expression of T-cell activation markers CD25, CD69, and CD44 in CD4⁺ T cells (Figure 11B), which is consistent with the previous findings in genetically PDK4-deleted CD4⁺ T cells (Figure 11C). In addition, treatment with GM-10395 decreased cytosolic calcium influx triggered by ATP/calcium-induced SOCE, as well as simultaneous mitochondrial calcium influx, in a dose-dependent manner (Figure 11C–F), which is consistent with the previous findings in PDK4 KO CD4⁺ T cells (Figure 10). Taken together with the absence of PDK4 (Figures 8–10), these data support the findings of compromised T-cell activation via abrogated intraorganelle calcium transfer between the ER and mitochondria upon PDK4 inhibition.

Remarkably, GM-10395 ameliorated both acute and chronic DSS-induced colitis, as evidenced by improved histology, preserved colon length, ameliorated intestinal permeability, and more rapid recovery of weight after DSS withdrawal (Figure 11G–V). Moreover, GM-10395-treated mice had significantly lower colonic transcription levels of *Ifng*, *Il6*, *Il12b*, *Il17a*, and *Tnfa* (Figure 11N). Collectively, these data demonstrate that pharmacologic inhibition of PDK4 by GM-10395 has therapeutic potential for IBD through compromised T-cell activation and mitochondria-ER calcium transfer in CD4⁺ T cells.

Discussion

We observed marked accumulation of PDK4- and p-PDHE1 α -positive CD4⁺ T cells in colon biopsy samples from patients with IBD. Furthermore, both genetic and pharmacologic approaches showed that PDK4 in T cells, but not in IECs, is required for colitis induction in an experimental colitis model. In vitro studies revealed that PDK4-deficient CD4⁺ T cells were less activated, with slowed metabolism,

as indicated by decreased OCR and ECAR, as well as by transcriptome analysis showing down-regulation of the glycolytic pathway,⁵ mitochondrial OXPHOS,⁴² and mTOR signaling.^{43,44} PDK4 deficiency resulted in a significant defect in Th17 differentiation but expanded Treg polarization, both in vitro and in vivo. Mechanistically, PDK4



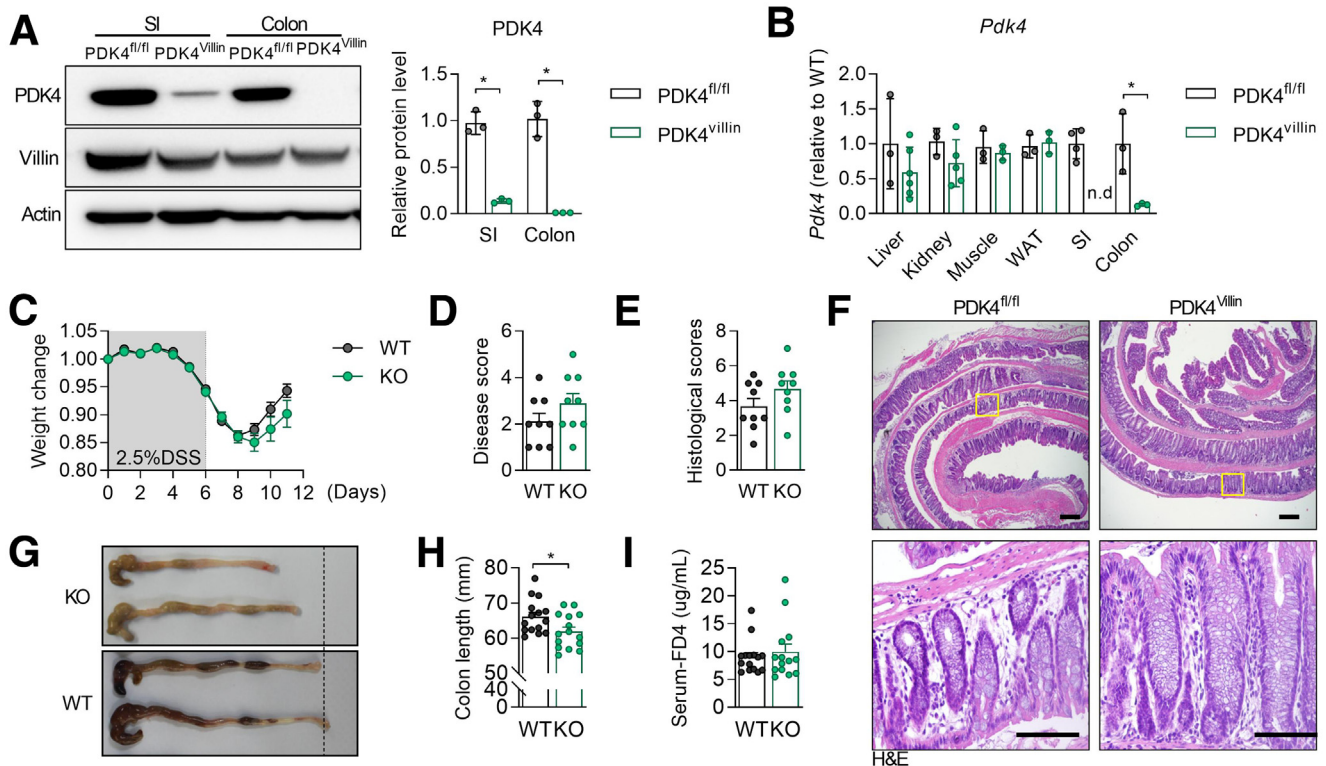


Figure 6. Deletion of PDK4 from IECs is not essential for protection against DSS-induced colitis. (A and B) Validation of PDK4^{Villin} mouse line. (A) Expression of PDK4 protein in intestinal epithelial cells (IECs) isolated from the small intestine (SI) and colon. (B) Levels of *Pdk4* transcripts in the liver, kidney, muscle, white adipose tissue (WAT), SI, and colon, as measured by qPCR. (C–I) PDK4^{fllox} (indicated as WT) and PDK4^{Villin} (indicated as KO) mice ($n = 6$) received 2.5% DSS in drinking water for 6 days. The experiment was repeated twice. (C) Weight changes. (D) Disease activity scores. (E) Representative images showing H&E staining of PDK4^{fllox} and PDK4^{Villin} after onset of DSS-induced colitis. (F) Histologic scores. (G) Gross images of the colon. (H) Colon length. (I) In vivo permeability test results after oral administration of FD4. Mean \pm standard error, Student *t* test: * $P < .05$.

deletion reduced SOCE, resulting in diminished cytosolic and mitochondrial calcium concentrations. Notably, consistent with our previous study in myotubes,¹⁹ we observed decreased MAM formation in PDK4-deficient CD4⁺ T cells, which is a plausible explanation for the disturbance in calcium homeostasis because MAM acts as a hub for calcium transfer between the ER and mitochondria.

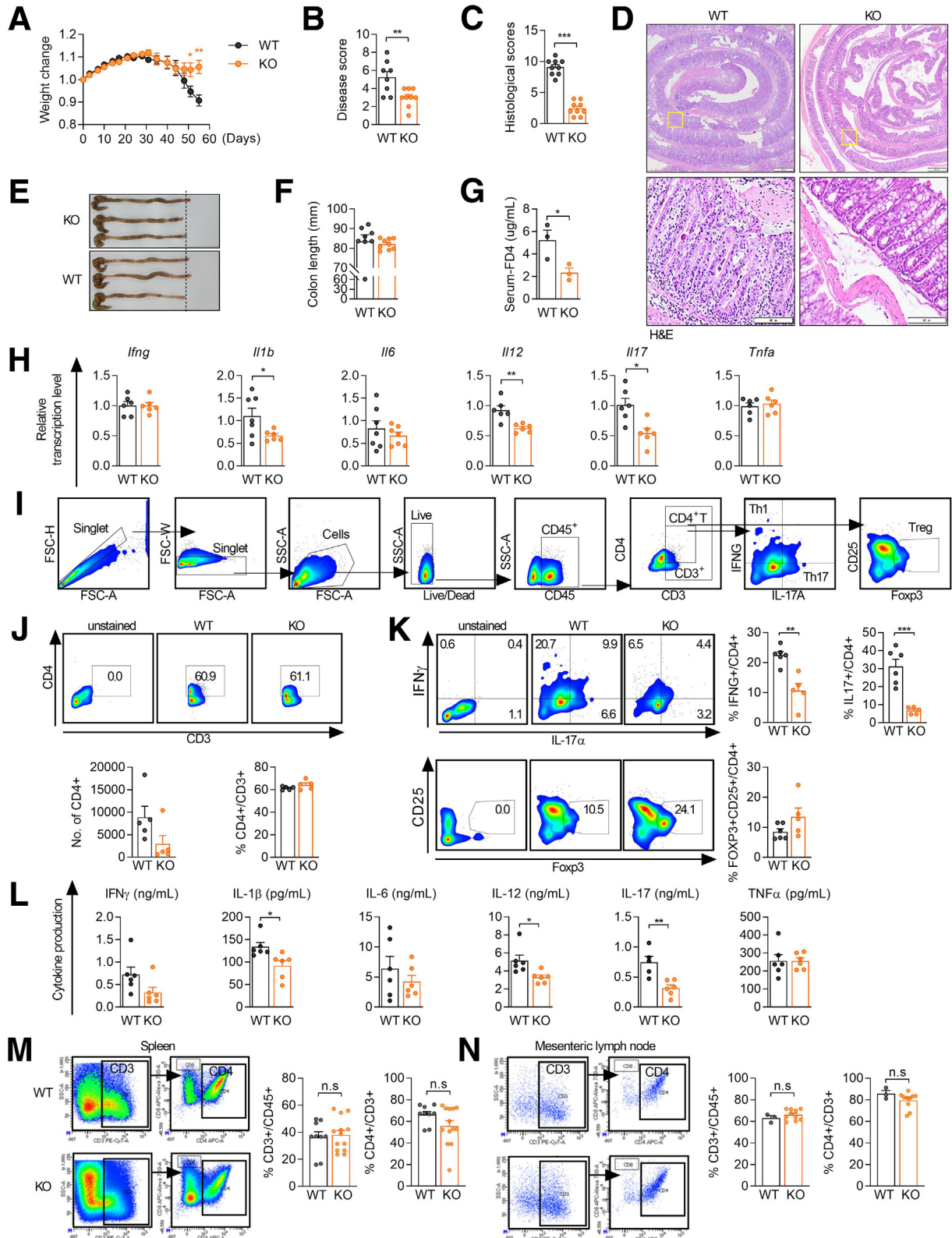
Traditionally, the well-recognized cellular functions of PDKs are achieved via PDH activation, which leads to reduction of glycolysis and increased OXPHOS.²¹ Previous studies show that PDK4-deficient cells exhibit increased PDH activity,^{25,45,46} which promotes OXPHOS within the

mitochondria²⁶ and suppresses aerobic glycolysis.^{47,48} T cells adopt metabolic reprogramming as a basis for “cellular decision making.” For example, metabolic reprogramming toward increased aerobic glycolysis and related transcription factors such as hypoxia-inducible factor 1 α ^{49,50} or c-Myc⁵ are critical for T-cell activation and proliferation.^{51,52} Because hypoxia-inducible factor 1 α or c-Myc is responsible for PDK transcription,^{53,54} it is thought that PDK is critically involved in T-cell metabolism. We observed a reduction in aerobic glycolysis in PDK4 KO T cells to some extent (Figure 5). Surprisingly, we noted a simultaneous reduction in the OCR in the absence of PDK4 (Figure 9G-K).

Figure 5. (See previous page). PDK4 deletion by CD4-Cre reduced intestinal inflammation in mice. (A–C) Validation of PDK4^{CD4} mouse line. (A) Expression of PDK4 protein in kidney, liver, and spleen samples from PDK4 WT PDK4^{fl/fl} or PDK4^{CD4} mice. (B) Relative protein expression was normalized to that of HSP90. (C) *Pdk4* (exon2) mRNA transcript levels in MACS-sorted CD4⁺ or CD4⁻ cells, as measured by quantitative PCR. (D–K) PDK4^{fl/fl} (denoted as WT) and PDK4^{CD4} (denoted as KO) mice ($n = 6$ –8/group) received 2.5% DSS in drinking water for 6 days. The experiment was repeated 3 times. (D) Weight changes. (E) Disease activity scores. (F) Histologic scores. (G) Representative H&E staining of tissues from PDK4^{fl/fl} and PDK4^{CD4} mice. Scale bars: upper, 500 μ m; lower, 100 μ m. (H) Gross image of the colon. (I) Colon length. (J) In vivo intestinal permeability test. (K) Relative expression of mRNA transcripts encoding *Ifng*, *Il1b*, *Il6*, *Il12b*, *Il17a*, and *Tnfa* in colonic tissues. (L) Gating strategy to identify Th1 (IFN- γ), Th17 (IL17 α), and Tregs (Foxp3⁺CD25⁺) cells ($n = 6$ mice/group). (M) Percentage of helper CD4⁺ T cells (CD4) among the CD3⁺ T-cell population in the lamina propria was measured by flow cytometry. (N) Flow cytometry analysis of percentage of Th1 (IFN- γ), Th17 (IL17 α), and Treg (Foxp3⁺CD25⁺) cells among gut-infiltrating CD4⁺ T cells. (O) Ex vivo cytokine production (IFN- γ , IL1 β , IL6, IL12, IL17, and TNF- α) of colon organ cultures was measured by ELISA ($n = 5$). Mean \pm standard error; * $P < .05$, ** $P < .01$, *** $P < .001$ (Student *t* test).

Although this is at least partially supported by a previous study that addressed the requirement for OXPHOS during T-cell activation,⁴² it remains unclear whether reduced

mitochondrial respiration due to PDK4 deficiency in CD4⁺ T cells is a cause or consequence of T-cell inactivation, and the underlying molecular mechanism is not evident.



Mitochondrial tricarboxylic acid cycle activity and the relevant OXPHOS pathway are dependent on mitochondrial calcium through calcium-sensitive dehydrogenases and ATPase.^{55,56} Mitochondrial calcium is critically regulated by crosstalk between ER and mitochondria called MAM.⁵⁷ Recently, we identified a noncanonical role of PDK4 in MAM formation and calcium homeostasis in skeletal muscle.¹⁹ A critical role of MAM in controlling mitochondria and effector function in memory CD8⁺ T cells was also identified.³⁰ On the basis of these previous findings, we asked whether PDK4 ablation in CD4⁺ T cells reduces calcium flux into mitochondria via the MAM structure. Indeed, we found that PDK4-deficient CD4⁺ T cells showed decreased MAM formation, which resulted in a subsequent reduction in mitochondrial calcium upon TCR-mediated activation (Figure 6D–F). Under this scenario in PDK4-deficient T cells, it is highly likely that reduction of mitochondrial calcium overrides canonical PDH activation during cell activation.

Mitochondrial calcium is required for optimal SOCE in T cells.^{10,58,59} However, the role of MAM in mitochondrial calcium and SOCE during T-cell activation is unclear. Previously, the effect of ER-mitochondrial MAM dissociation on SOCE was demonstrated in fibroblasts. Knockdown of neuronal calcium sensor 1 impairs IP3R-induced mitochondrial calcium uptake by fibroblasts through ER-mitochondrial calcium transport, resulting in modest impairment of both SOCE and mitochondrial respiration.⁶⁰ In line with this, we showed that PDK4 inhibition dampens ER-mitochondrial crosstalk, mitochondrial calcium transfer, and SOCE in CD4⁺ T cells (Figure 6).

Furthermore, we showed that PDK4 inhibition subsequently blocks translocation of calcineurin-dependent NFAT to the nucleus of CD4⁺ T cells (Figure 6H). This observation is in line with the previous finding that inhibition of the mitochondrial calcium uniporter attenuates SOCE and NFAT activation in a rat leukemia cell line.⁶¹ Another article shows that disruption of mitochondria-ER calcium crosstalk via deletion of thioredoxin-related transmembrane protein 1/3 in melanoma cells also inhibits calcineurin and translocation of NFAT to the nucleus.⁶² Therefore, regulation of mitochondrial calcium appears to be critical for NFAT activation in CD4⁺ T cells.

Calcium signaling induced by SOCE is highly associated with metabolic reprogramming during T-cell activation, differentiation,^{10,11,41} and pathogenicity.⁶³ Ablation of SOCE by

STIM deletion significantly reduces calcineurin-dependent NFATc1 activation⁶⁴ and, in turn, decreases transcriptional expression of glycolytic enzymes in activated T cells.⁴¹ Accordingly, STIM1 deficiency markedly attenuates development of pathogenic Th17 cells by compromising mitochondrial gene expression and mitochondrial reactive oxygen species production, thereby preventing development of colitis.⁶³ These results are in line with another report showing that SOCE ablation by deletion of ORAI suppresses SOCE and causes defective T-cell differentiation.¹⁰ In this study, we showed that PDK4 inhibition significantly compromised transcription of glycolytic enzymes containing an NFAT-binding motif (Figure 5), thereby decreasing aerobic glycolysis in activated T cells (Figure 9). In addition, PDK4 inhibition mitigated Th17 differentiation in vivo and in vitro. Collectively, the data suggest that PDK4 inhibition is a viable strategy for resolving immune responses by pathogenic CD4⁺ T cells.

We also demonstrated robust metabolic reprogramming toward aerobic glycolysis by measuring p-PDHE1 α in some of LP-infiltrating leukocytes using a DSS-induced colitis model. These cells include not only CD4⁺ T cells but also neutrophils and macrophages (Figure 1G). Although we focused on the role of PDK4 in CD4⁺ T-cell activation by metabolic reprogramming and mitochondria-ER calcium transfer, we cannot rule out the possibility that PDK4 deficiency in macrophages or neutrophils has anticollitogenic effects in mice. Previous studies show that expression of PDK4 is up-regulated significantly in LPS-treated⁶⁵ or lipopolysaccharide/IFN- γ -treated macrophages.²⁵ As expected, inhibition of PDK4 significantly decreased lipopolysaccharide-induced glycolysis burst and increased expression of anti-inflammatory IL10.⁶⁵ Even PDK2/PDK4 double deficiency synergistically compromises hypoxia-inducible factor 1 α expression in macrophages.²⁵ Treatment with dichloroacetate, a pan-PDK inhibitor, mirrors PDK4 or PDK2/4 deletion in activated macrophages.^{25,65} Moreover, neutrophils depend substantially on aerobic glycolysis and on the pentose phosphate pathway for their immune functions,⁶⁶ as shown by several inhibitor studies,^{67,68} despite lack of direct evidence that PDKs are involved.

Collectively, our findings demonstrate that suppressing PDK4 attenuates activation of pathogenic CD4⁺ T cells by metabolic reprogramming via MAM/calcium-dependent

Figure 7. (See previous page). PDK4-deficient T cells delay intestinal homing and induction of colitis after adoptive transfer. *Rag1*^{-/-} mice received 4×10^5 CD4⁺CD45RB^{hi}CD25⁻ T cells sorted from splenocytes isolated from WT or PDK4 KO mice (n = 9). The experiment was repeated 3 times. (A) Weight changes. (B) Disease activity scores. (C) Histologic scores. (D) Representative H&E staining of tissues from PDK4^{fl/fl} and PDK4^{CD4} mice. Scale bars: upper, 500 μ m; lower, 100 μ m. (E) Gross image of the colon. (F) Colon length. (G) In vivo intestinal permeability test. (H) Relative expression of mRNA transcripts encoding *Ifng*, *Il1b*, *Il6*, *Il12b*, *Il17a*, and *Tnfa* in colon tissues (n = 6). (I) Gating strategy to identify Th1 (IFN- γ), Th17 (IL17 α), and Tregs (Foxp3⁺CD25⁺) cells (n = 6 mice/group). (J) Percentage of helper CD4⁺ T cells (CD4) among the CD3⁺ T-cell population in the lamina propria was measured by flow cytometry. (K) Flow cytometry analysis of percentage of Th1 (IFN- γ), Th17 (IL17 α), and Treg (Foxp3⁺CD25⁺) cells among gut-infiltrating CD4⁺ T cells. (L) Ex vivo cytokine production (IFN- γ , IL1 β , IL6, IL12, IL17, and TNF- α) of colon organ cultures was measured by ELISA (n = 6). Mean \pm standard error; *P < .05, **P < .01, ***P < .001 (Student t test). (M and N) Natural Treg-depleted naive CD4⁺ T cells (CD4⁺CD45RB^{hi}CD25⁻) were transferred to *Rag1*^{-/-} mice. Samples were collected from the spleen and mesenteric lymph nodes and subjected to flow cytometry analysis to investigate whether PDK4 KO T cells show normal survival, proliferation, and tissue-homing capacity in secondary lymphoid organs [(M) spleen and (N) mesenteric lymph nodes] in vivo.

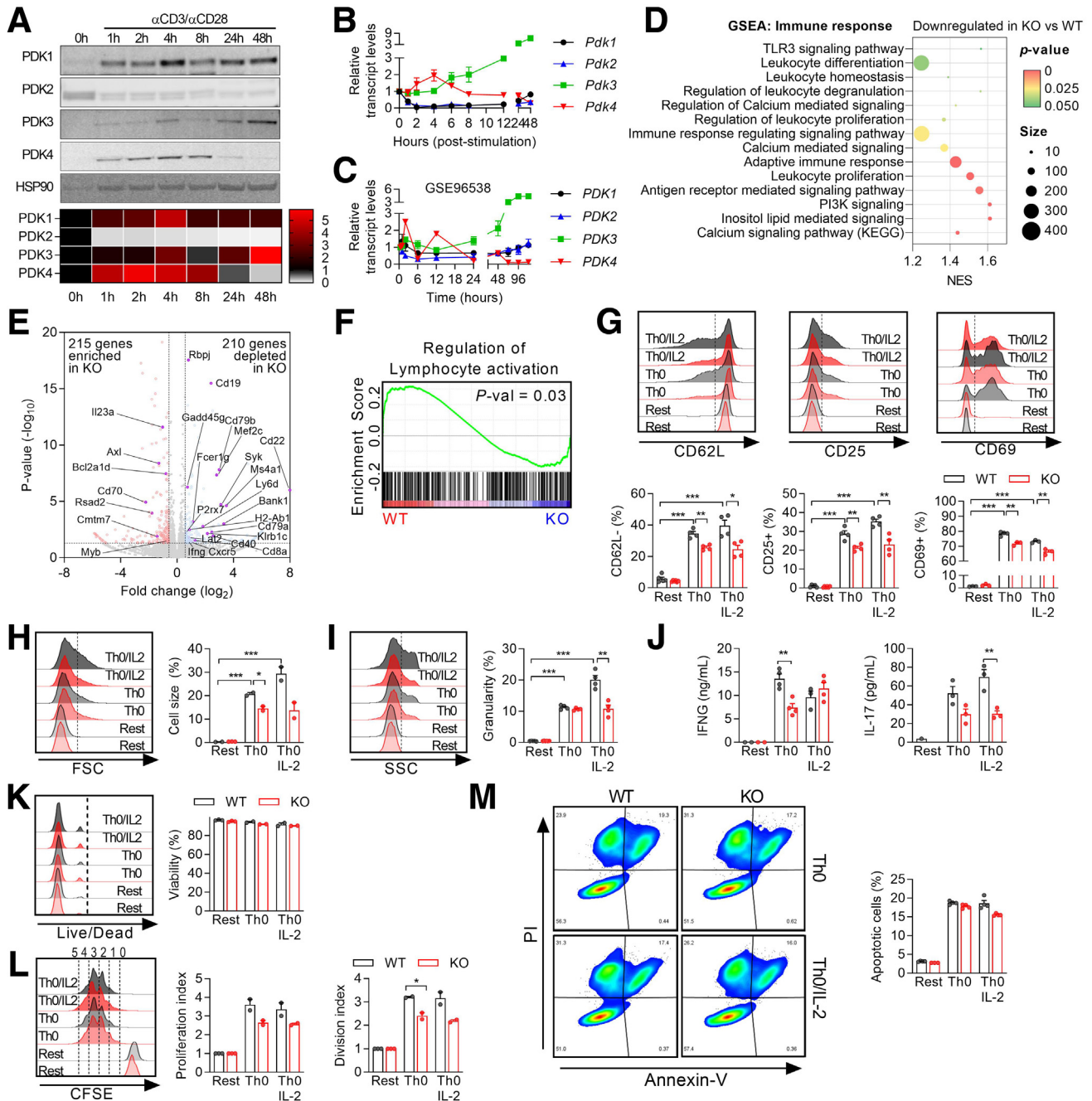


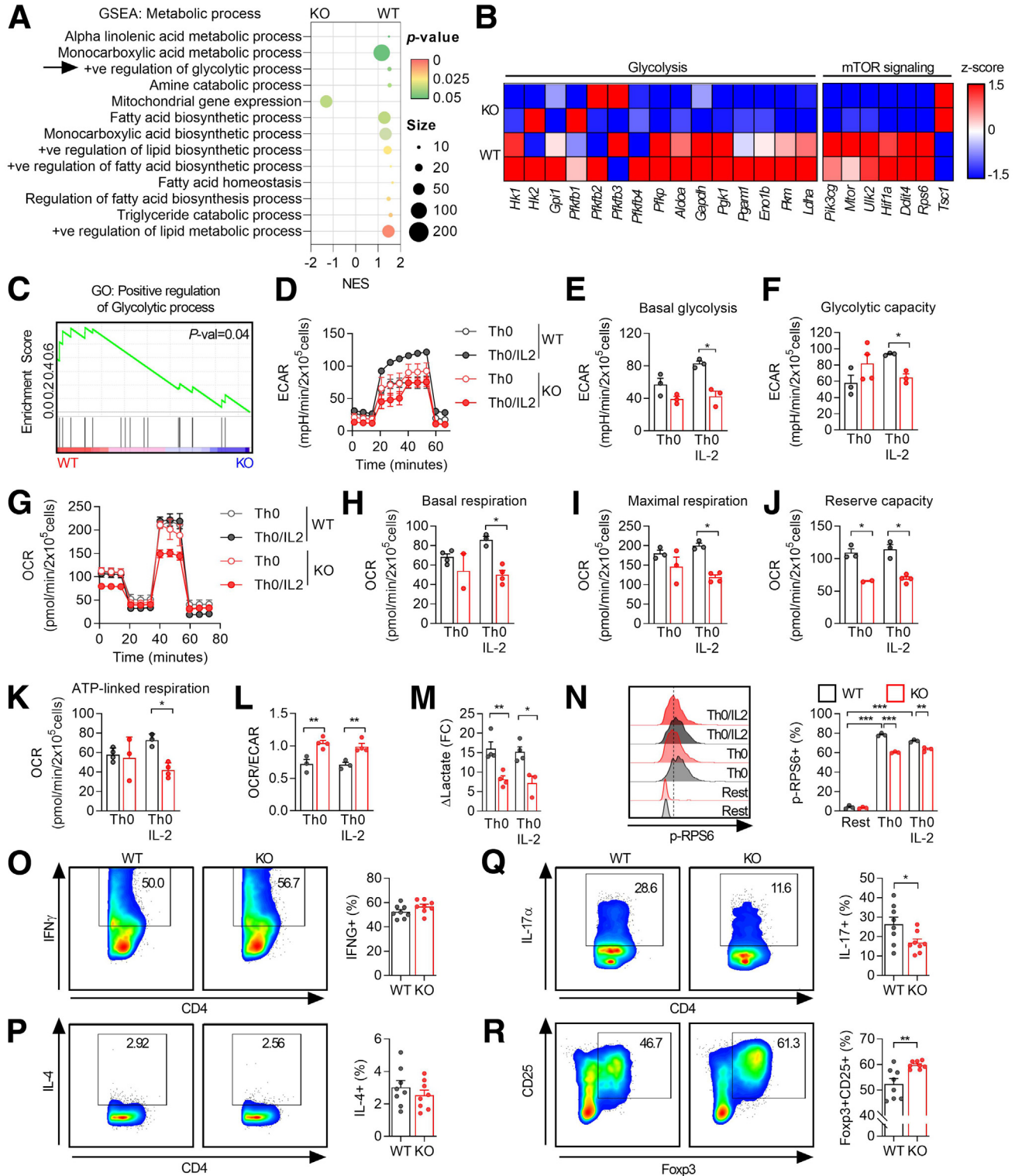
Figure 8. PDK4 differentially regulates expression of genes associated with T-cell activation. (A and B) WT naive CD4⁺ T cells were treated with α CD3 and α CD28 for 0, 1, 2, 4, 8, 24, and 48 hours. The fold changes in protein and mRNA expression of each PDK1-4 isotype were measured by Western blotting and qPCR, respectively. (C) Meta-analysis of PDK transcript levels in human WT naive CD4⁺ T cells after TCR-induced activation based on previously published gene expression data sets (GSE96538). Expression levels were normalized to T = 2 hours. (D) WT or PDK4 KO naive CD4⁺ T cells were activated for 48 hours under Th0 conditions. Scatter plot of Gene Set Enrichment Analysis (GSEA) using a gene set of interest (immune response on C2:KEGG or C2:BIOCARTA pathway database). (E) Next-generation sequencing identified 425 differentially expressed genes (DEGs). Volcano plot showing DEGs based on the following cutoff setting (P value < .05; fold change > 1.5). Overall, 210 genes were down-regulated and 215 were up-regulated in KO T cells. DEGs associated with lymphocyte activation (GO:0046649) were labeled. (F) GSEA of genes involved in regulation of lymphocyte activation (GO:0051249). (G) PDK4 WT or KO naive CD4⁺ T cells were stimulated for 3 days under Th0 conditions in presence/absence of IL2 ($n = 4$). T-cell activation makers (CD62L⁺, CD25⁺, CD69⁺) were analyzed by flow cytometry. The experiment was repeated twice. (H–M) Naive CD4⁺ PDK4 WT or KO T cells were activated for 72 hours ($n = 2-3$). (H) Cell size, as assessed by forward scatter (FSC), and (I) cell granularity, as assessed by side scatter (SSC). (J) Secreted IFN- γ and IL17 α were measured in sandwich ELISAs. Viability, proliferation, and apoptosis were evaluated by (K) Live/Dead staining, (L) CFSE staining, and (M) PI/Annexin V staining. This experiment was repeated at least twice. Mean \pm standard error, Student t test: * $P < .05$, ** $P < .01$, *** $P < .001$.

pathways. These results provide convincing evidence that PDK4 is a potential novel therapeutic target for management of IBD. Future studies examining whether PDK4 inhibitors can be applied to human IBD are anticipated.

Materials and Methods

Mice

PDK4 KO mice (B6.129-Pdk4tm1Rhar/J), provided by Dr Robert A. Harris (Indiana University School of Medicine),



were backcrossed to WT C57BL/6J mice for at least 8 generations. Littermates were used as controls in all experiments. *Rag1*^{-/-} mice (B6.129S7-*Rag1*^{tm1Mom}/J) were purchased from the Jackson Laboratory. CD4^{Cre/+} mice (B6.Cg-TgCd4-cre1Cwi/BfluJ), provided by Dr Gap R. Lee (Sogang University, South Korea), and Villin^{Cre/+} mice (B6.Cg-TgVil1-cre997Gum/J), provided by Dr Mi N. Kweon (University of Ulsan College of Medicine/Asan Medical Center, South Korea), were used to generate PDK4^{CD4} and PDK4^{Villin} mice, respectively, by crossing with PDK4^{fl/fl} mice (Cyagen Biosciences, Suzhou, China). C57BL/6J Jms1c mice were used for the pharmacologic inhibition test. All mice were housed in a specific pathogen-free and temperature-controlled room (12:12 hours light/dark cycle).

Patients

Mucosal biopsies were collected from 24 patients with newly diagnosed IBD (11, UC; 13, CD) and from 6 non-IBD healthy controls at Kyungpook National University Hospital. No patients were taking corticosteroids or biologic treatments. Forceps biopsies of inflamed and noninflamed mucosa, as assessed by colonoscopy, were taken.

DSS-induced Colitis Model

Acute colitis was induced in male mice to exclude possible effects of hormonal differences or menstrual cycle. Eight-week-old male mice received 2.5% DSS (MP Bio-medicals, Irvine, CA) in sterile drinking water ad libitum for 6 days, followed by normal drinking water for 5 days unless otherwise indicated.

Adoptive T-Cell Transfer in the Colitis Model

CD4⁺ T cells were enriched from splenocytes using an EasySep Mouse CD4⁺ T Cell Isolation Kit (cat. no. 19852; STEMCELL Technologies, Vancouver, Canada). To induce colitis, male *Rag1*^{-/-} mice (6–7 weeks old) were infused (intraperitoneally) with 4×10^5 naive CD4⁺ T cells (CD4⁺CD45RB^{hi}CD25⁻) in sterile phosphate-buffered saline (PBS). CD4⁺CD45RB^{hi}CD25⁻ cells were sorted using a MoFlo XDP cell sorter (Beckman Coulter, Brea, CA) or FACSAria III (BD Biosciences).

Assessment of Colitis

Mice were monitored daily or weekly for body weight loss and signs of intestinal inflammation. The disease

activity score is a semiquantitative score calculated as the sum of stool consistency scores, occult blood scores, and weight loss scores.⁶⁹ To analyze intestinal epithelial permeability in vivo, mice were administered oral fluorescein isothiocyanate–dextran 4 kDa (FD4) 46944 (Sigma-Aldrich, St Louis, MO) in sterile saline. Blood was collected after 4 hours by cardiac puncture, and serum FD4 was measured with a fluorescence spectrophotometer at λ_{em} 488 nm/ λ_{ex} 520 nm. For some experiments, colon length was measured and compared between groups. Disease severity was examined histopathologically using a previously published scoring system,⁷⁰ for which the criteria include loss of goblet cells, crypt abscesses, cellular infiltration, mucosa elongation, and epithelial erosion.

In Vitro Culture of Naive T Cells

Naive CD4⁺ T cells were isolated using a mouse CD4⁺CD62L⁺ T Cell Isolation Kit 130-106-643 (Miltenyi Biotec, Bergisch Gladbach, Germany). The purity was checked by flow cytometry analysis (>92%). Naive CD4⁺ T cells were cultured in RPMI medium (Welgene, Gyeongsan, South Korea) at 37°C for 2–3 days with plate-bound anti-CD3 and anti-CD28 antibodies under Th0 conditions (10% fetal bovine serum, 1% penicillin-streptomycin, and 2.5 μ mol/L mercaptoethanol, in the presence or absence of 50 U/mL IL2).

RNA-Sequencing

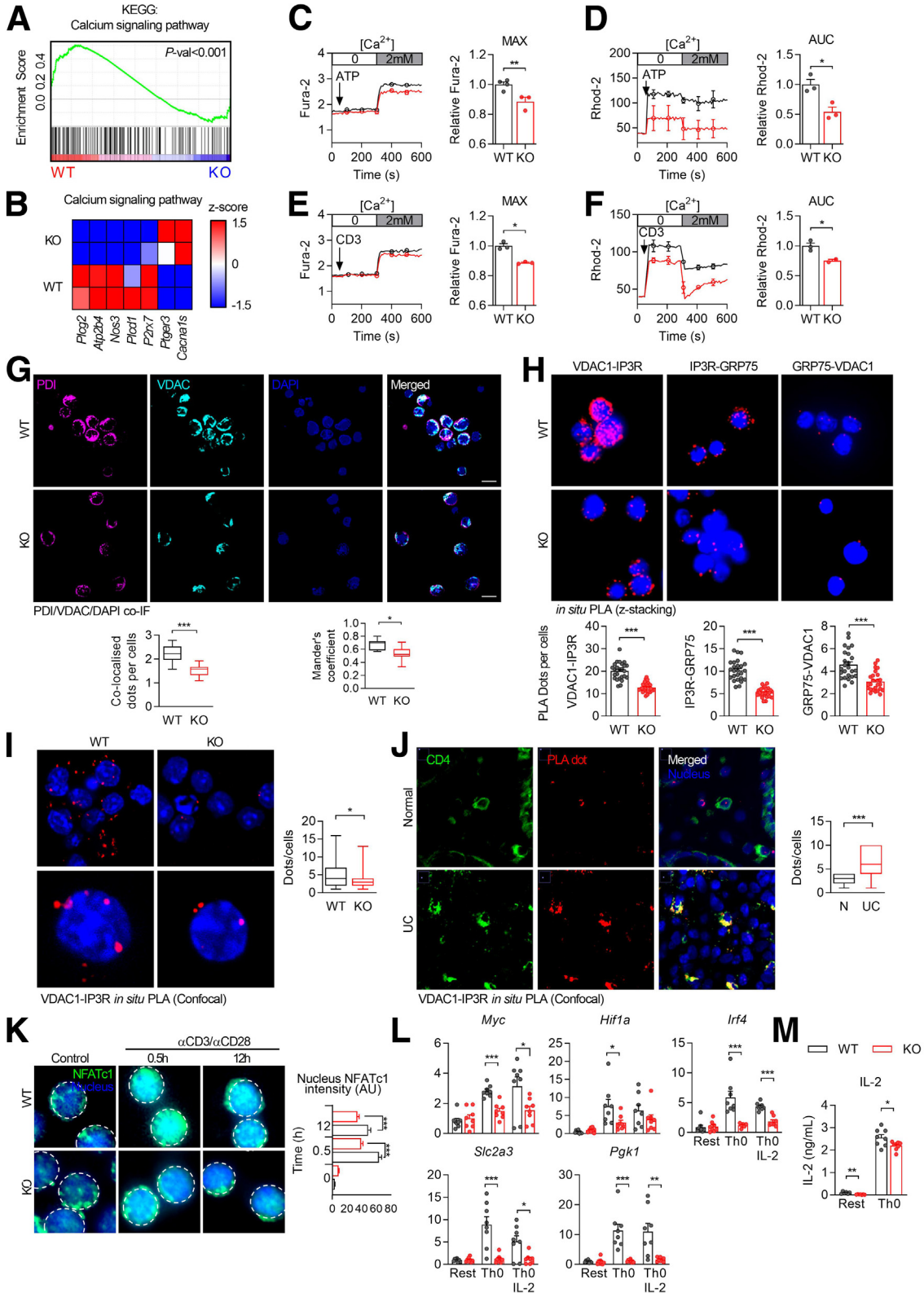
Isolated naive CD4⁺ T cells were activated for 2 days in vitro, as described above. Total mRNA was extracted from 2,000,000 cells using Trizol (Qiagen, Hilden, Germany). Samples with RNA integrity number >6.1 and DV200 >50% were used to generate a library of reasonable quality using Quant-Seq 3' mRNA-Seq Library Prep Kits. Because Quant-Seq specifically targets the 3' end of transcripts, even RNAs with a lower RIN are suitable as input material. The amplified library was sequenced using a HiSeq 2500 System (Illumina, San Diego, CA). To compare differential gene expression, DESeq2 (Bioconductor v3.3.0) in R studio was used.⁷¹ GSEA was performed using the Broad Institute tool GSEA v4.0.3.⁷² Test gene sets included the C2.CP.KEGG and C5.BP gene sets from the Molecular Signatures Database. All data, including expression profiles generated in this study, are available through the Gene Expression Omnibus (accession no. GSE161653).

Figure 9. (See previous page). PDK4 mediates metabolic reprogramming of activated CD4⁺ T cells and T-cell differentiation. (A) Scatter plot of Gene Set Enrichment Analysis (GSEA) results using a gene set of interest (metabolic process on C2:KEGG or C2:BIOCARTA pathway database). (B) Heatmap showing expression of genes associated with glycolytic enzymes and the mTOR signaling pathway. (C) GSEA plot showing genes involved in positive regulation of glycolytic processes (Gene set GO:0045821). (D–F) WT or PDK4 KO CD4⁺ T cells were stimulated for 3 days under Th0 conditions. (D) Glycolysis stress test assessed using an XF96 analyzer. The experiment was repeated 3 times. (E) Basal glycolysis measured in glycolysis stress test. (F) Glycolytic capacity was measured in glycolysis stress test. (G) Oxygen consumption rate was measured in mitochondrial stress test. (H–K) Basal OCR, maximal OCR, reserve capacity OCR, and ATP-linked OCR were calculated on basis of the mitochondrial stress test. (L) Ratio of basal OCR to basal ECAR. (M) Relative amounts of cytosolic lactate were measured by liquid chromatography–mass spectrometry. (N) Frequency of phosphorylated ribosomal protein S6 (p-RPS6) was analyzed by flow cytometry (n = 3). (O–R) PDK4 WT or KO naive CD4⁺ T cells were differentiated for 2 days under (O) Th1, (P) Th2, (Q) Th17, or (R) Treg polarizing conditions. Each T-cell subsets were identified by flow cytometry analysis. The experiment was repeated 3 times. Mean \pm standard error, Student *t* test: **P* < .05, ***P* < .01, ****P* < .001.

Measurement of Intracellular Calcium

Naive CD4⁺ T cells were incubated for 40 minutes with 2.5 mmol/L Fura-2-AM or Rhod-2-AM (Thermo Fisher

Scientific, Waltham, MA). After washing, cells were kept in calcium-free Hanks balanced salt solution. Intracellular or mitochondrial calcium levels were measured using



FlexStation 3 (Molecular Devices, San Jose, CA). After 1 minute, ATP (300 $\mu\text{mol/L}$) or CD3 (10 $\mu\text{g/mL}$) was added to induce depletion of ER calcium stores. Calcium influx was initiated by addition of calcium-containing Hanks balanced salt solution (final concentration, 2 mmol/L).

Flow Cytometry Analysis

For intracellular staining of phosphor-proteins, cells were fixed with 2% paraformaldehyde, followed by permeabilization in 95% methanol. The following antibodies were used: anti-p-PDHE1 α (AP1062; Calbiochem, Darmstadt, Germany) and a fluorescein isothiocyanate conjugated antirabbit secondary antibody (Santa Cruz Biotechnology, Dallas, TX). For staining of intracellular cytokines/transcription factors, either the Mouse Foxp3 Buffer Set 560409 (BD Biosciences, Franklin Lakes, NJ) or the Foxp3/Transcription Factor Staining Buffer Set 00-5523-00 (eBioscience, San Diego, CA) was used along with the following antibodies: CD45-BV421, CD3-PECy7, CD4-APC, CD8-Alexafluor700, NK1.1-BV711, IFN- γ -BV510, IL-4-BV605, IL-17-PerCP-Cy5.5, CD25-BV785, Foxp3-FITC, CD69-PerCP-Cy5.5, and CD62L-PerCP-Cy5.5 (all from BioLegend, San Diego, CA). Cell viability was measured using a Live/Dead staining kit (Thermo Fisher). Cell death was measured using an FITC/Annexin V Apoptosis Detection Kit (556547; BD Biosciences).

Western Blot Analysis

Protein samples (20 μg) were separated in premade NuPAGE Bis-Tris gels (Thermo Fisher) and transferred to polyvinylidene difluoride membranes. The following antibodies were used: anti-PDK1 ADI-KAP-PK112-D (Enzo Biochem, New York, NY), anti-PDK2 sc-100534 (Santa Cruz Biotechnology), anti-PDK3 serum (rabbit antiserum provided by Dr Robert A Harris), anti-PDK4 ab214938 (Abcam, Cambridge, MA), anti-p-PDHE1 α (Calbiochem, San Diego, CA), anti-HSP90 #4874 (Cell Signaling Technology, Danvers, MA), and anti- β -actin A5441 (Sigma-Aldrich). Proteins were visualized using an LAS-4000 (BD Biosciences) or iBright1500 (Thermo Fisher).

Quantitative Polymerase Chain Reaction

Total RNA was extracted using Trizol reagent (Qiagen), and a RevertAid First Strand cDNA Synthesis Kit (Thermo Fisher) was used to generate a cDNA library. Quantitative real-time polymerase chain reaction (qPCR) was performed using Power SYBR Green PCR Master Mix (Applied Biosystems, Waltham, MA) and a ViiA 7 Real-time PCR system (Applied Biosystems). The primers used in this study are listed in Table 1.

Immunohistochemistry

Formalin-fixed paraffin-embedded sections were rehydrated by immersing the slides in xylene for 4 minutes (twice), 100% ethanol for 2 minutes (twice), 95% ethanol for 2 minutes (twice), 80% ethanol for 2 minutes (twice), 70% ethanol for 2 minutes (twice), and PBS for 5 minutes (twice). Epitope retrieval was performed in IHC-Tek Epitope Retrieval Solution IW-1100 (IHC World, Elliott, MD). The slides were blocked with 5% bovine serum albumin and stained with the following antibodies: PDK4 (Novus), p-PDHE1 α , Ki-67, anti-CD4-PECy7, anti-CD3-PECy7 (all BioLegend), and goat antirabbit immunoglobulin G conjugated to Alexa Fluor 647 (A27040; Invitrogen, Carlsbad, CA).

Measurement of Secreted Cytokines

Secreted IFN- γ and IL17 were measured using sandwich Quantikine enzyme-linked immunosorbent assay (ELISA) kits (all from R&D systems, Minneapolis, MN). Secreted IL2 was measured using an IL-2 Mouse ELISA kit (Invitrogen).

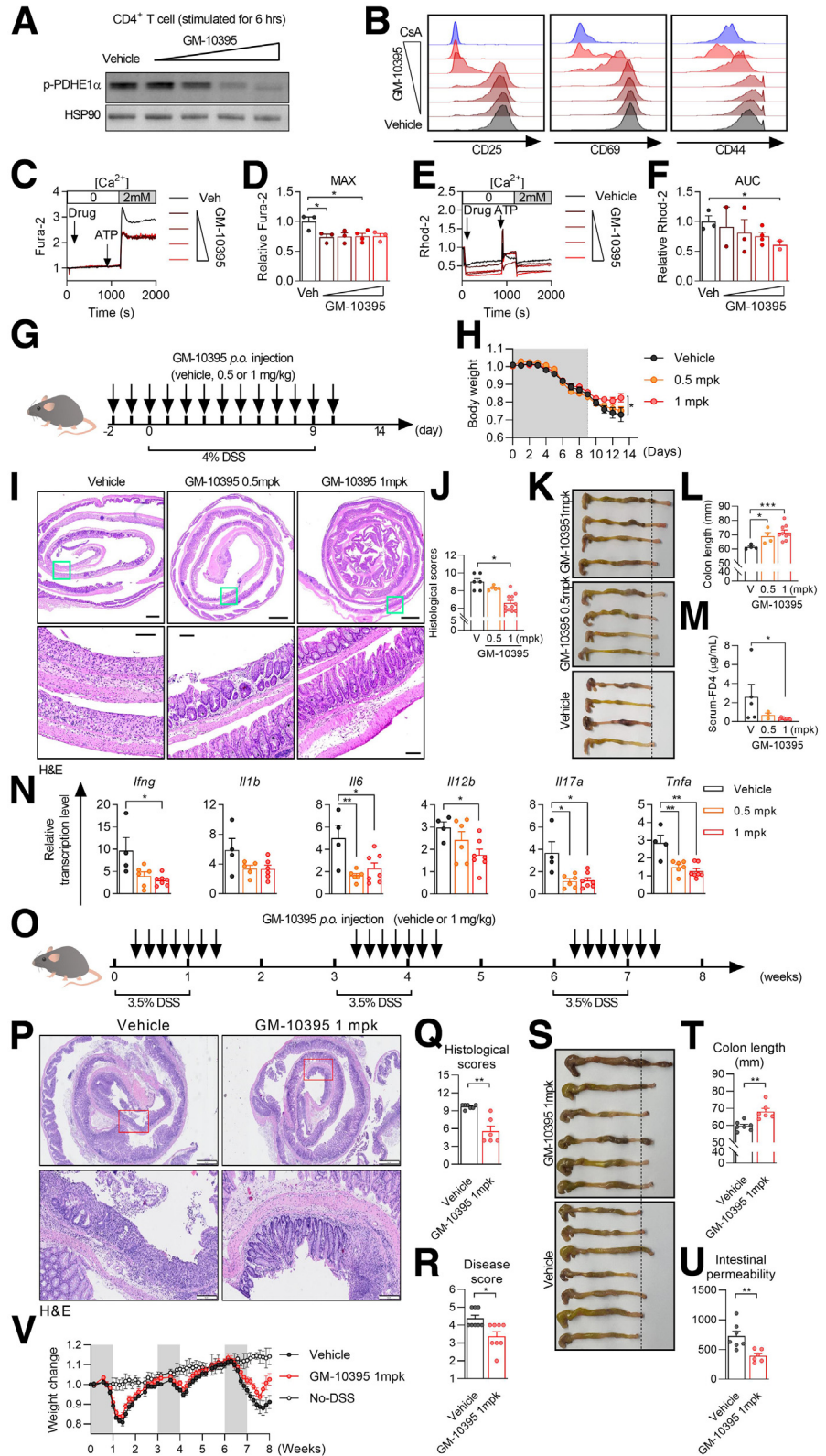
Ex Vivo Intestinal Organ Culture

The colon was placed in sterile ice-cold PBS, and luminal contents were removed by flushing with ice-cold PBS. The colon tissues were then opened longitudinally and washed thoroughly with ice-cold PBS. Approximately 1 cm of the middle part of the colon was excised using a scissors and incubated in RPMI medium supplemented with 10% fetal bovine serum, 1% P/S, and protease inhibitor cocktail P1860 (Sigma-Aldrich) for 24 hours at 37°C. The amounts of secreted cytokines were measured using ELISA kits (Invitrogen).

Figure 10. (See previous page). MAM/SOCE/NFAT pathway is compromised by PDK4 deletion in activated CD4⁺ T cells. (A) GSEA plot of genes involved in the calcium signaling pathway (KEGG). (B) Heatmap of DEGs associated with the KEGG calcium signaling pathways. (C–F) Cytosolic and mitochondrial calcium were measured using Fura-2 and Rhod-2, respectively (n = 3). This experiment was repeated twice. IP3R-mediated calcium release from ER of naive CD4⁺ T cells from PDK4 WT or KO mice was induced by ATP (C and D) or α CD3 (E and F). Later, extracellular calcium (2 mmol/L) was added to induce SOCE. (G) Mitochondria-ER colocalization was visualized by co-immunofluorescence staining. CD4⁺ T cells from PDK4 WT or KO naive were activated for 3 days under Th0 conditions. Co-immunofluorescence staining of ER (PDI, magenta), mitochondria (VDAC, cyan), and nuclei (DAPI, blue). Scale bar, 10 μm . Mander's coefficient was measured by ImageJ. (H and I) Mitochondria-ER colocalization was also visualized by in situ proximity ligation assay (PLA) (red dots). WT or PDK4 KO CD4⁺ T cells activated by α CD3 + α CD28 + IL2 for 72 hours. Nuclei were stained with DAPI (blue). (H) Representative in situ PLA z-stacked images of VDAC1-IP3R, IP3R-GRP75, or GRP75-VDAC1. (I) Representative confocal images of in situ PLA (red dots) of VDAC1/IP3R. Mean \pm standard error; * P < .05, ** P < .01, *** P < .001 (Mann-Whitney test). (J) MAM is enriched in gut-infiltrating CD4 T cells from patients with UC (n = 10) compared with normal controls (n = 5); in situ PLA of VDAC1/IP3R (red) co-stained with hCD4 (green). Nuclei are stained with DAPI (blue). Mean \pm standard error, Student t test: *** P < .001. (K) Localization of NFATc1 (green) upon α CD3/ α CD28 stimulation for 0.5 or 12 hours. Nuclei are stained with DAPI (blue and dashed line). (L) Relative transcription of glycolytic enzymes or transcriptional regulators bearing an NFAT-binding motif. (M) Secreted IL2 was measured in sandwich ELISA. Mean \pm standard error; * P < .05, ** P < .01, *** P < .001 (Mann-Whitney test).

Figure 11. Pharmacologic inhibition of PDK4 inhibits T-cell activation and SOCE in CD4⁺ T cells and prevents acute/chronic DSS-induced colitis.

(A) Effects of GM-10395 (0.5, 1, 5, and 10 $\mu\text{mol/L}$) on dephosphorylation of PDHE1 α in activated CD4⁺ T cells cultured for 6 hours under Th0/IL-2 conditions. The experiment was repeated twice. (B) Naive CD4⁺ T cells were activated under Th0/IL2 conditions and co-treated with GM-10395 (1, 5, 10, 20, and 50 $\mu\text{mol/L}$) for 72 hours. T-cell activation markers (CD25⁺, CD69⁺, and CD44⁺) were measured by flow cytometry. Cyclosporin A (CsA; 10 $\mu\text{g/ml}$) was used as a positive control for T-cell inactivation. The experiment was repeated twice. (C–F) Effects of GM-10395 (0.1, 0.3, 1, and 3 $\mu\text{mol/L}$) on ATP-triggered SOCE. Cytosolic and mitochondrial calcium levels were measured by Fura-2 (C and D) and Rhod-2 (E and F), respectively. The experiment was repeated twice. Mean \pm standard error; * $P < .05$, ** $P < .01$, *** $P < .001$ (Mann-Whitney test). (G) C57BL/6J JmsSlc mice ($n = 6$) received 4% DSS in drinking water for 9 days. GM-10395 (0.5 or 1 mg per kg) was administered orally. The experiment was repeated twice. (H) Body weight. (I) Representative images of H&E staining. (J) Histologic scores. (K) Gross image of the colon. (L) Colon length. (M) Permeability test results after oral administration of FD4. (N) Relative expression of mRNA transcripts encoding *Iifng*, *Ii1b*, *Ii6*, *Ii12b*, *Ii17a*, and *Tnfa* in colonic tissues. (O) C57BL6J JmsSlc mice ($n = 7-8$) were treated with 3 cycles of DSS. GM-10395 (1 mg/kg) was administered orally for 1 week, beginning after 3 days of DSS treatment. Mice were anesthetized for colitis examination. (P) H&E staining. (Q) Histologic scores were evaluated to determine disease severity. (R) Disease scores. (S) Gross image of the colon. (T) Colon length. (U) In vivo intestinal permeability. (V) Weight changes. Mean \pm standard error; * $P < .05$, ** $P < .01$, *** $P < .001$ (Student *t* test).



In Situ Proximity Ligation Assay

In situ proximity ligation assay was performed according to the instructions for the Duolink in situ PLA kit (Sigma-

Aldrich). Anti-VDAC1, anti-IP3R1, or anti-GRP75 antibodies were used to visualize MAM formation. Fluorescent blobs were detected using a FV1000 confocal laser scanning

Table 1. List of Primers Used in This Study

Gene	Forward	Reverse
<i>Ifng</i>	3'-CAGCAACAGCAAGGCGAAAA-5'	3-TGGACCTGTGGGTTGTTGAC-5';
<i>Tnfa</i>	3-AGCCGATGGGTTGTACCTTG-5'	3-ATAGCAAATCGGCTGACGGT-5';
<i>Il6</i>	3-CTTGGGACTGATGCTGGTGA-5'	3-GGTCTGTTGGGAGTGGTATCC-5';
<i>Il1b</i>	3-GAGCACCTTCTTTTCTTCATCTT-5'	3-TCACACACCAGCAGTTATCATC-5';
<i>Il12b</i>	3-TTGCCATCGTTTTGCTGGTG-5'	3-CACTGTTTCTCCAGGGGCAT-5';
<i>Il17</i>	3-TCCTGGTCTGAAGAGGGAG-5'	3-CACACCCACCAGCATCTTCT-5';
<i>Reg3g</i>	3-TTCCTGTCCTCCATGATCAAAA-5'	3-CATCCACCTCTGTTGGGTTCA-5';
<i>Muc1</i>	3-TCTTTCCAACCCAGGACACC-5'	3-ACTGCCATTACCTGCCGAAA-5'
<i>Muc2</i>	3-AGAAGCCAGATCCCGAAACC-5'	3-GGGAATCGGTAGACATCGCC-5';
<i>Kit</i>	3-GTCCTGTTGGTCTGCTCC-5'	3-TGTGCTGGATGGATGGATGG-5';
<i>Lgr5</i>	3-ATCTCCTGTCGCTTCCCT-5'	3-CTGTAAGGCTCGGTTCCCTG-5';
<i>Myc</i>	3-TGTGGAGAAGAGGCCAAACCC-5'	3-GTTGTGCTGGTGGTGGAGA-5'
<i>Hif1a</i>	3-TGTTCCAGAGGGAGCCAAAA-5'	3-GTTATGAACCTGCTGGGCTG-5'
<i>Irf4</i>	3-TATGCCACGATTGGAGCAGG-5'	3-GAAAACGGAGCAAACAGCCA-5'
<i>Slc2a4</i>	3-GTCGTGATGAGGGTGGACTT-5'	3-TTGCTCCATTGTCCAAGCA-5'
<i>Pgk1</i>	3-TGAAGTGTGGGAAAACGGGG-5'	3-AGCCAGAAATCGGTGGTGT-5'

biological microscope (Olympus, Tokyo, Japan) or an ImageXpress Micro Confocal Imaging System (Molecular Devices). The number of detected blobs per nucleus was calculated by ImageJ software or MetaMorph Microscopy Software (Molecular Devices).

Cellular Bioenergetics Respiration Analysis Using the Extracellular Flux Analyzer

Activated naive CD4⁺ T cells were added to CellTak-coated XF96-well plates at 200,000 cells/well. Mitochondrial stress and glycolysis stress tests were performed using an eXF96 analyzer (Agilent Technologies, Santa Clara, CA) according to the manufacturer's instructions.

In Vitro T-Cell Differentiation

Mouse naive CD4⁺ T cells were differentiated for 3 days into Th1, Th2, Th17, or Treg cells using CellXVivo Lymphocyte Differentiation Kits CDK018, CDK019, CDK017, or CDK007 (R&D Systems), respectively.

Pharmacologic Inhibition of PDK4

C57BL/6J JmsSlc WT male mice were exposed to 4% DSS in drinking water for 9 days ad libitum. GM-10395, a novel inhibitor of PDK4, was administered at 0.5 or 1 mg/kg daily by oral gavage from day -2 to 10 (13 days in total). No adverse effects were observed at this dose (data not shown). In vitro assay of GM-10395 was performed as described previously.⁷³ Cyclosporin A (Enzo Life Sciences), a calcineurin inhibitor, was used as a positive control. To induce chronic colitis, we administered 3 cycles of 3.5% DSS in sterile drinking water ad libitum for 1 week, followed by normal drinking water for 2 weeks. After the last cycle, mice were killed 1 week after return to normal drinking water. GM-10395 (1 mg/kg daily) was

administered from day 3 after DSS challenge (and continued for 1 week).

Statistical Analysis

The Student *t* test or the Mann-Whitney test was performed in Prism5 (GraphPad, La Jolla, CA) or Excel (Microsoft, Redmond, WA). The Pearson coefficient and Mander's coefficient were calculated by ImageJ (National Institutes of Health, Bethesda, MD). Error bars represent the mean ± standard error of the mean. *P* values of <.05, <.01, or <.001 are indicated by 1, 2, or 3 asterisks, respectively, in all figures.

Study Approval

All animal experiments were approved by the Institutional Animal Care and Use Committee (IACUC) of Daegu-Gyeongbuk Medical Innovation Foundation, South Korea (DGMIF-19070201-00) and by the IACUC of Kyungpook National University (KNU-2021-0080). The present human study was reviewed and approved by the Institutional Review Board of Kyungpook National University Hospital (KNUH-2017-10-034). All patients provided informed consent.

References

1. Sartor RB. Mechanisms of disease: pathogenesis of Crohn's disease and ulcerative colitis. *Nat Clin Pract Gastroenterol Hepatol* 2006;3:390-407.
2. Shin B, Kress RL, Kramer PA, Darley-Usmar VM, Bellis SL, Harrington LE. Effector CD4 T cells with progenitor potential mediate chronic intestinal inflammation. *J Exp Med* 2018;215:1803-1812.
3. Maynard CL, Weaver CT. Intestinal effector T cells in health and disease. *Immunity* 2009;31:389-400.

4. Smids C, Horjus Talabur Horje CS, Drylewicz J, Roosenboom B, Groenen MJM, van Koolwijk E, van Lochem EG, Wahab PJ. Intestinal T cell profiling in inflammatory bowel disease: linking T cell subsets to disease activity and disease course. *J Crohns Colitis* 2018; 12:465–475.
5. Wang R, Dillon CP, Shi LZ, Milasta S, Carter R, Finkelstein D, McCormick LL, Fitzgerald P, Chi H, Munger J, Green DR. The transcription factor Myc controls metabolic reprogramming upon T lymphocyte activation. *Immunity* 2011;35:871–882.
6. Donnelly RP, Finlay DK. Glucose, glycolysis and lymphocyte responses. *Mol Immunol* 2015;68(Pt C):513–519.
7. Shi LZ, Wang R, Huang G, Vogel P, Neale G, Green DR, Chi H. HIF1alpha-dependent glycolytic pathway orchestrates a metabolic checkpoint for the differentiation of TH17 and Treg cells. *J Exp Med* 2011;208:1367–1376.
8. Park YJ, Yoo SA, Kim M, Kim WU. The role of calcium-calcieneurin-NFAT signaling pathway in health and autoimmune diseases. *Frontiers in Immunology* 2020;11:195.
9. Trebak M, Kinet JP. Calcium signalling in T cells. *Nat Rev Immunol* 2019;19:154–169.
10. Vaeth M, Yang J, Yamashita M, Zee I, Eckstein M, Knosp C, Kaufmann U, Karoly Jani P, Lacruz RS, Flockerzi V, Kacs Kovics I, Prakriya M, Feske S. ORAI2 modulates store-operated calcium entry and T cell-mediated immunity. *Nature Communications* 2017;8:14714.
11. McCarl CA, Khalil S, Ma J, Oh-hora M, Yamashita M, Roether J, Kawasaki T, Jairaman A, Sasaki Y, Prakriya M, Feske S. Store-operated Ca²⁺ entry through ORAI1 is critical for T cell-mediated autoimmunity and allograft rejection. *J Immunol* 2010;185:5845–5858.
12. Bertin S, Aoki-Nonaka Y, de Jong PR, Nohara LL, Xu H, Stanwood SR, Srikanth S, Lee J, To K, Abramson L, Yu T, Han T, Touma R, Li X, Gonzalez-Navajas JM, Herdman S, Corr M, Fu G, Dong H, Gwack Y, Franco A, Jefferies WA, Raz E. The ion channel TRPV1 regulates the activation and proinflammatory properties of CD4(+) T cells. *Nature Immunology* 2014;15:1055–1063.
13. Bertin S, Aoki-Nonaka Y, Lee J, de Jong PR, Kim P, Han T, Yu T, To K, Takahashi N, Boland BS, Chang JT, Ho SB, Herdman S, Corr M, Franco A, Sharma S, Dong H, Akopian AN, Raz E. The TRPA1 ion channel is expressed in CD4+ T cells and restrains T-cell-mediated colitis through inhibition of TRPV1. *Gut* 2017;66:1584–1596.
14. Holness MJ, Kraus A, Harris RA, Sugden MC. Targeted upregulation of pyruvate dehydrogenase kinase (PDK)-4 in slow-twitch skeletal muscle underlies the stable modification of the regulatory characteristics of PDK induced by high-fat feeding. *Diabetes* 2000;49:775–781.
15. Sugden MC, Holness MJ. Therapeutic potential of the mammalian pyruvate dehydrogenase kinases in the prevention of hyperglycaemia. *Curr Drug Targets Immune Endocr Metabol Disord* 2002;2:151–165.
16. Jeoung NH, Harris CR, Harris RA. Regulation of pyruvate metabolism in metabolic-related diseases. *Rev Endocr Metab Disord* 2014;15:99–110.
17. Jha MK, Lee IK, Suk K. Metabolic reprogramming by the pyruvate dehydrogenase kinase-lactic acid axis: linking metabolism and diverse neuropathophysiology. *Neurosci Biobehav Rev* 2016;68:1–19.
18. Park BY, Jeon JH, Go Y, Ham HJ, Kim JE, Yoo EK, Kwon WH, Jeoung NH, Jeon YH, Koo SH, Kim BG, He L, Park KG, Harris RA, Lee IK. PDK4 deficiency suppresses hepatic glucagon signaling by decreasing cAMP levels. *Diabetes* 2018;67:2054–2068.
19. Thoudam T, Ha CM, Leem J, Chanda D, Park JS, Kim HJ, Jeon JH, Choi YK, Liangpunsakul S, Huh YH, Kwon TH, Park KG, Harris RA, Park KS, Rhee HW, Lee IK. PDK4 augments ER-mitochondria contact to dampen skeletal muscle insulin signaling during obesity. *Diabetes* 2019;68:571–586.
20. Zhang M, Zhao Y, Li Z, Wang C. Pyruvate dehydrogenase kinase 4 mediates lipogenesis and contributes to the pathogenesis of nonalcoholic steatohepatitis. *Biochem Biophys Res Commun* 2018;495:582–586.
21. Park S, Jeon JH, Min BK, Ha CM, Thoudam T, Park BY, Lee IK. Role of the pyruvate dehydrogenase complex in metabolic remodeling: differential pyruvate dehydrogenase complex functions in metabolism. *Diabetes & Metabolism Journal* 2018;42:270–281.
22. Lee JM, Kim MJ, Lee SJ, Kim BG, Choi JY, Lee SM, Ham HJ, Koh JM, Jeon JH, Lee IK. PDK2 deficiency prevents ovariectomy-induced bone loss in mice by regulating the RANKL-NFATc1 pathway during osteoclastogenesis. *J Bone Miner Res* 2021;36:553–566.
23. Rahman MH, Bhusal A, Kim JH, Jha MK, Song GJ, Go Y, Jang IS, Lee IK, Suk K. Astrocytic pyruvate dehydrogenase kinase-2 is involved in hypothalamic inflammation in mouse models of diabetes. *Nature Communications* 2020;11:5906.
24. Kang HJ, Min BK, Choi WI, Jeon JH, Kim DW, Park S, Lee YK, Kim HJ, Byeon JE, Go Y, Ham HJ, Jeon YH, Kim MJ, Lee JY, Wende AR, Choi SH, Harris RA, Lee IK. Pyruvate dehydrogenase kinase 1 and 2 deficiency reduces high-fat diet-induced hypertrophic obesity and inhibits the differentiation of preadipocytes into mature adipocytes. *Exp Mol Med* 2021;53:1390–1401.
25. Min BK, Park S, Kang HJ, Kim DW, Ham HJ, Ha CM, Choi BJ, Lee JY, Oh CJ, Yoo EK, Kim HE, Kim BG, Jeon JH, Hyeon DY, Hwang D, Kim YH, Lee CH, Lee T, Kim JW, Choi YK, Park KG, Chawla A, Lee J, Harris RA, Lee IK. Pyruvate dehydrogenase kinase is a metabolic checkpoint for polarization of macrophages to the M1 phenotype. *Frontiers in Immunology* 2019;10:944.
26. Oh CJ, Ha CM, Choi YK, Park S, Choe MS, Jeoung NH, Huh YH, Kim HJ, Kweon HS, Lee JM, Lee SJ, Jeon JH, Harris RA, Park KG, Lee IK. Pyruvate dehydrogenase kinase 4 deficiency attenuates cisplatin-induced acute kidney injury. *Kidney Int* 2017;91:880–895.
27. Raturi A, Simmen T. Where the endoplasmic reticulum and the mitochondrion tie the knot: the mitochondria-associated membrane (MAM). *Biochim Biophys Acta* 2013;1833:213–224.
28. Bravo R, Gutierrez T, Paredes F, Gatica D, Rodriguez AE, Pedrozo Z, Chiong M, Parra V, Quest AF, Rothermel BA, Lavandero S. Endoplasmic reticulum: ER stress regulates mitochondrial bioenergetics. *Int J Biochem Cell Biol* 2012;44:16–20.

29. Krols M, Bultynck G, Janssens S. ER-mitochondria contact sites: a new regulator of cellular calcium flux comes into play. *J Cell Biol* 2016;214:367–370.
30. Bantug GR, Fischer M, Grahlert J, Balmer ML, Unterstab G, Develioglu L, Steiner R, Zhang L, Costa ASH, Gubser PM, Burgener AV, Sauder U, Loliger J, Belle R, Dimeloe S, Lotscher J, Jauch A, Recher M, Honger G, Hall MN, Romero P, Frezza C, Hess C. Mitochondria-endoplasmic reticulum contact sites function as immunometabolic hubs that orchestrate the rapid recall response of memory CD8(+) T cells. *Immunity* 2018;48:542–555 e6.
31. Neurath MF. Cytokines in inflammatory bowel disease. *Nat Rev Immunol* 2014;14:329–342.
32. te Velde AA, de Kort F, Sterrenburg E, Pronk I, ten Kate FJ, Hommes DW, van Deventer SJ. Comparative analysis of colonic gene expression of three experimental colitis models mimicking inflammatory bowel disease. *Inflamm Bowel Dis* 2007;13:325–330.
33. Mottet C, Uhlig HH, Powrie F. Cutting edge: cure of colitis by CD4+CD25+ regulatory T cells. *J Immunol* 2003;170:3939–3943.
34. Mizoguchi E, Low D, Ezaki Y, Okada T. Recent updates on the basic mechanisms and pathogenesis of inflammatory bowel diseases in experimental animal models. *Intestinal Research* 2020;18:151–167.
35. Schmidt A, Marabita F, Kiani NA, Gross CC, Johansson HJ, Elias S, Rautio S, Eriksson M, Fernandes SJ, Silberberg G, Ullah U, Bhatia U, Lahdesmaki H, Lehtio J, Gomez-Cabrero D, Wiendl H, Lahesmaa R, Tegner J. Time-resolved transcriptome and proteome landscape of human regulatory T cell (Treg) differentiation reveals novel regulators of FOXP3. *BMC Biol* 2018;16:47.
36. Chi H. Regulation and function of mTOR signalling in T cell fate decisions. *Nat Rev Immunol* 2012;12:325–338.
37. Pearce EL, Poffenberger MC, Chang CH, Jones RG. Fueling immunity: insights into metabolism and lymphocyte function. *Science* 2013;342:1242454.
38. Martinvalet D. The role of the mitochondria and the endoplasmic reticulum contact sites in the development of the immune responses. *Cell Death Dis* 2018;9:336.
39. Ferris CD, Hagan RL, Snyder SH. Calcium flux mediated by purified inositol 1,4,5-trisphosphate receptor in reconstituted lipid vesicles is allosterically regulated by adenine nucleotides. *Proc Natl Acad Sci U S A* 1990; 87:2147–2151.
40. Yang R, Liang BT. Cardiac P2X(4) receptors: targets in ischemia and heart failure? *Circ Res* 2012;111:397–401.
41. Vaeth M, Maus M, Klein-Hessling S, Freinkman E, Yang J, Eckstein M, Cameron S, Turvey SE, Serfling E, Berberich-Siebelt F, Possemato R, Feske S. Store-operated Ca(2+) entry controls clonal expansion of T cells through metabolic reprogramming. *Immunity* 2017; 47:664–679 e6.
42. Chang CH, Curtis JD, Maggi LB Jr, Faubert B, Villarino AV, O'Sullivan D, Huang SC, van der Windt GJ, Blagih J, Qiu J, Weber JD, Pearce EJ, Jones RG, Pearce EL. Posttranscriptional control of T cell effector function by aerobic glycolysis. *Cell* 2013;153:1239–1251.
43. Delgoffe GM, Pollizzi KN, Waickman AT, Heikamp E, Meyers DJ, Horton MR, Xiao B, Worley PF, Powell JD. The kinase mTOR regulates the differentiation of helper T cells through the selective activation of signaling by mTORC1 and mTORC2. *Nature Immunology* 2011;12:295–303.
44. Jones RG, Pearce EJ. MENTORing immunity: mTOR signaling in the development and function of tissue-resident immune cells. *Immunity* 2017;46:730–742.
45. Lee SJ, Jeong JY, Oh CJ, Park S, Kim JY, Kim HJ, Doo Kim N, Choi YK, Do JY, Go Y, Ha CM, Choi JY, Huh S, Ho Jeoung N, Lee KU, Choi HS, Wang Y, Park KG, Harris RA, Lee IK. Pyruvate dehydrogenase kinase 4 promotes vascular calcification via SMAD1/5/8 phosphorylation. *Sci Rep* 2015;5:16577.
46. Zhao Z, Ji M, Wang Q, He N, Li Y. miR-16-5p/PDK4-mediated metabolic reprogramming is involved in chemoresistance of cervical cancer. *Molecular Therapy Oncolytics* 2020;17:509–517.
47. Jha MK, Song GJ, Lee MG, Jeoung NH, Go Y, Harris RA, Park DH, Kook H, Lee IK, Suk K. Metabolic connection of inflammatory pain: pivotal role of a pyruvate dehydrogenase kinase-pyruvate dehydrogenase-lactic acid axis. *J Neurosci* 2015;35:14353–14369.
48. Stacpoole PW, Greene YJ. Dichloroacetate. *Diabetes Care* 1992;15:785–791.
49. Finlay DK, Rosenzweig E, Sinclair LV, Feijoo-Carnero C, Hukelmann JL, Rolf J, Panteleyev AA, Okkenhaug K, Cantrell DA. PDK1 regulation of mTOR and hypoxia-inducible factor 1 integrate metabolism and migration of CD8+ T cells. *J Exp Med* 2012;209:2441–2453.
50. Dang EV, Barbi J, Yang HY, Jinasena D, Yu H, Zheng Y, Bordman Z, Fu J, Kim Y, Yen HR, Luo W, Zeller K, Shimoda L, Topalian SL, Semenza GL, Dang CV, Pardoll DM, Pan F. Control of T(H)17/T(reg) balance by hypoxia-inducible factor 1. *Cell* 2011;146:772–784.
51. Macintyre AN, Gerriets VA, Nichols AG, Michalek RD, Rudolph MC, Deoliveira D, Anderson SM, Abel ED, Chen BJ, Hale LP, Rathmell JC. The glucose transporter Glut1 is selectively essential for CD4 T cell activation and effector function. *Cell Metabolism* 2014;20:61–72.
52. Palmer CS, Ostrowski M, Balderson B, Christian N, Crowe SM. Glucose metabolism regulates T cell activation, differentiation, and functions. *Front Immunol* 2015;6:1.
53. Jung GS, Jeon JH, Choi YK, Jang SY, Park SY, Kim SW, Byun JK, Kim MK, Lee S, Shin EC, Lee IK, Kang YN, Park KG. Pyruvate dehydrogenase kinase regulates hepatitis C virus replication. *Sci Rep* 2016;6:30846.
54. Lee JH, Kim EJ, Kim DK, Lee JM, Park SB, Lee IK, Harris RA, Lee MO, Choi HS. Hypoxia induces PDK4 gene expression through induction of the orphan nuclear receptor ERRgamma. *PLoS One* 2012;7:e46324.
55. Rizzuto R, De Stefani D, Raffaello A, Mammucari C. Mitochondria as sensors and regulators of calcium signalling. *Nat Rev Mol Cell Biol* 2012;13:566–578.
56. Territo PR, Mootha VK, French SA, Balaban RS. Ca(2+) activation of heart mitochondrial oxidative phosphorylation: role of the F(0)/F(1)-ATPase. *Am J Physiol Cell Physiol* 2000;278:C423–C435.
57. Rizzuto R, Pinton P, Carrington W, Fay FS, Fogarty KE, Lifshitz LM, Tuft RA, Pozzan T. Close contacts with the

- endoplasmic reticulum as determinants of mitochondrial Ca²⁺ responses. *Science* 1998;280:1763–1766.
58. Quintana A, Schwindling C, Wenning AS, Becherer U, Rettig J, Schwarz EC, Hoth M. T cell activation requires mitochondrial translocation to the immunological synapse. *Proc Natl Acad Sci U S A* 2007; 104:14418–14423.
 59. Hoth M, Button DC, Lewis RS. Mitochondrial control of calcium-channel gating: a mechanism for sustained signaling and transcriptional activation in T lymphocytes. *Proc Natl Acad Sci U S A* 2000;97:10607–10612.
 60. Angebault C, Fauconnier J, Patergnani S, Rieusset J, Danese A, Affortit CA, Jagodzinska J, Megy C, Quiles M, Cazevieille C, Korchagina J, Bonnet-Wersinger D, Milea D, Hamel C, Pinton P, Thiry M, Lacampagne A, Delprat B, Delettre C. ER-mitochondria cross-talk is regulated by the Ca(2+) sensor NCS1 and is impaired in Wolfram syndrome. *Sci Signal* 2018;11.
 61. Samanta K, Douglas S, Parekh AB. Mitochondrial calcium uniporter MCU supports cytoplasmic Ca²⁺ oscillations, store-operated Ca²⁺ entry and Ca²⁺-dependent gene expression in response to receptor stimulation. *PLoS One* 2014;9:e101188.
 62. Zhang X, Gibhardt CS, Will T, Stanisz H, Korbel C, Mitkovski M, Stejerean I, Cappello S, Pacheu-Grau D, Dudek J, Tahbaz N, Mina L, Simmen T, Laschke MW, Menger MD, Schon MP, Helms V, Niemeyer BA, Rehling P, Vultur A, Bogeski I. Redox signals at the ER-mitochondria interface control melanoma progression. *EMBO J* 2019;38:e100871.
 63. Kaufmann U, Kahlfuss S, Yang J, Ivanova E, Korolov SB, Feske S. Calcium signaling controls pathogenic Th17 cell-mediated inflammation by regulating mitochondrial function. *Cell Metabolism* 2019;29:1104–1118 e6.
 64. Oh-Hora M, Yamashita M, Hogan PG, Sharma S, Lamperti E, Chung W, Prakriya M, Feske S, Rao A. Dual functions for the endoplasmic reticulum calcium sensors STIM1 and STIM2 in T cell activation and tolerance. *Nature Immunology* 2008;9:432–443.
 65. Na YR, Jung D, Song J, Park JW, Hong JJ, Seok SH. Pyruvate dehydrogenase kinase is a negative regulator of interleukin-10 production in macrophages. *Journal of Molecular Cell Biology* 2020;12:543–555.
 66. Jeon JH, Hong CW, Kim EY, Lee JM. Current understanding on the metabolism of neutrophils. *Immune Network* 2020;20:e46.
 67. Azevedo EP, Rochael NC, Guimaraes-Costa AB, de Souza-Vieira TS, Ganihio J, Saraiva EM, Palhano FL, Foguel D. A metabolic shift toward pentose phosphate pathway is necessary for amyloid fibril- and phorbol 12-myristate 13-acetate-induced neutrophil extracellular trap (NET) formation. *J Biol Chem* 2015; 290:22174–22183.
 68. Rodriguez-Espinosa O, Rojas-Espinosa O, Moreno-Altamirano MM, Lopez-Villegas EO, Sanchez-Garcia FJ. Metabolic requirements for neutrophil extracellular traps formation. *Immunology* 2015;145:213–224.
 69. Xu Y, Hunt NH, Bao S. The role of granulocyte macrophage-colony-stimulating factor in acute intestinal inflammation. *Cell Res* 2008;18:1220–1229.
 70. Chinen T, Komai K, Muto G, Morita R, Inoue N, Yoshida H, Sekiya T, Yoshida R, Nakamura K, Takayanagi R, Yoshimura A. Prostaglandin E2 and SOCS1 have a role in intestinal immune tolerance. *Nature Communications* 2011;2:190.
 71. Love MI, Huber W, Anders S. Moderated estimation of fold change and dispersion for RNA-seq data with DESeq2. *Genome Biol* 2014;15:550.
 72. Subramanian A, Tamayo P, Mootha VK, Mukherjee S, Ebert BL, Gillette MA, Paulovich A, Pomeroy SL, Golub TR, Lander ES, Mesirov JP. Gene set enrichment analysis: a knowledge-based approach for interpreting genome-wide expression profiles. *Proc Natl Acad Sci U S A* 2005;102:15545–15550.
 73. Lee D, Pagire HS, Pagire SH, Bae EJ, Dighe M, Kim M, Lee KM, Jang YK, Jaladi AK, Jung KY, Yoo EK, Gim HE, Lee S, Choi WI, Chi YI, Song JS, Bae MA, Jeon YH, Lee GH, Liu KH, Lee T, Park S, Jeon JH, Lee IK, Ahn JH. Discovery of novel pyruvate dehydrogenase kinase 4 inhibitors for potential oral treatment of metabolic diseases. *J Med Chem* 2019;62:575–588.

Received March 17, 2022. Accepted September 29, 2022.

Correspondence

Address correspondence to: Eun Soo Kim, MD, PhD, Division of Gastroenterology, Department of Internal Medicine, School of Medicine, Kyungpook National University, 130 Dongdeok-ro, Jung-gu, Daegu, Republic of Korea 41944. e-mail: dandy813@hanmail.net; fax: +82-53-200-5879 OR In-Kyu Lee, MD, PhD, Department of Internal Medicine, School of Medicine, Kyungpook National University, 130 Dongdeok-ro, Jung-gu, Daegu, Republic of Korea 41944. e-mail: leei@knu.ac.kr.

Acknowledgments

The authors thank Gap R. Lee (Sogang University, South Korea), Mi N. Kweon (University of Ulsan College of Medicine/Asan Medical Center, South Korea), and Robert A. Harris (Indiana University School of Medicine) for providing genetically modified animals.

CRedit Authorship Contributions

Hoyul Lee (Conceptualization: Equal; Methodology: Lead; Software: Lead; Formal analysis: Lead; Investigation: Equal; Data Curation: Lead; Writing – original draft preparation: Equal; Visualization: Lead; Funding acquisition: Supporting)

Jaeh Han Jeon (Conceptualization: Equal; Formal analysis: Supporting; Writing – original draft preparation: Equal; Funding acquisition: Supporting)

Yu-Jeong Lee (Formal analysis: Supporting; Investigation: Equal; Data Curation: Supporting)

Mi-Jin Kim (Formal analysis: Supporting; Investigation: Supporting)

Woong Hee Kwon (Investigation: Supporting)

Dipanjana Chanda (Writing – original draft preparation: Supporting)

Themis Thoudam (Writing – original draft preparation: Supporting)

Haushabh S. Pagire (Resources: Equal)

Suvarna H. Pagire (Resources: Equal)

Jun Hee Ahn (Resources: Equal)

Robert A. Harris (Resources: Equal)

Eun Soo Kim (Conceptualization: Equal; Writing – original draft preparation: Equal; Supervision: Equal; Resources: Equal; Funding acquisition: Equal)

In-Kyu Lee (Conceptualization: Equal; Supervision: Equal; Funding acquisition: Equal)

Conflicts of interest

The authors disclose no conflicts.

Funding

Supported by the Korea Health Technology R&D Project, through the Korea Health Industry Development Institute (KHIDI), funded by the Ministry of Health & Welfare, Republic of Korea (HI16C1501 and HR22C1832); the Basic Science Research Program, through the National Research Foundation (NRF) of Korean government (MSIT) (NRF-2017R1A2B3006406, NRF-2020R1C1C1012729, NRF-2017R1D1A1B03028512, and NRF-2020R1C1C1009322); and the Bio & Medical Technology Development Program of the NRF, funded by the Korean government (MSIP&MOHW) (NRF-2016M3A9B6902872).